VYSOKÉ UČENÍ TECHNICKÉ V BRNĚ

BRNO UNIVERSITY OF TECHNOLOGY

FAKULTA STROJNÍHO INŽENÝRSTVÍ
ÚSTAV FYZIKÁLNÍHO INŽENÝRSTVÍ

FACULTY OF MECHANICAL ENGINEERING
INSTITUTE OF PHYSICAL ENGINEERING

PŘÍPRAVA A ANALÝZA NANOSTRUKTUR V PODMÍNKÁCH UHV

BAKALÁŘSKÁ PRÁCE

BACHELOR'S THESIS

AUTOR PRÁCE JONÁŠ GLOSS

AUTHOR

BRNO 2012

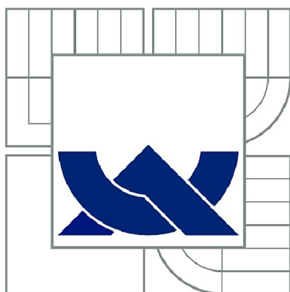

VYSOKÉ UČENÍ TECHNICKÉ V BRNĚ

BRNO UNIVERSITY OF TECHNOLOGY

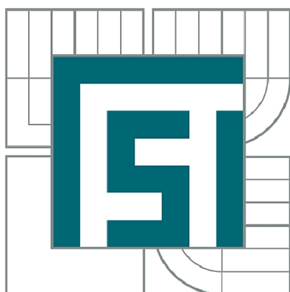

FAKULTA STROJNÍHO INŽENÝRSTVÍ
ÚSTAV FYZIKÁLNÍHO INŽENÝRSTVÍ

FACULTY OF MECHANICAL ENGINEERING
INSTITUTE OF PHYSICAL ENGINEERING

PŘÍPRAVA A ANALÝZA NANOSTRUKTUR V PODMÍNKÁCH UHV

PREPARATION AND ANALYSIS OF NANOSTRUCTURES IN UHV CONDITIONS

BAKALÁŘSKÁ PRÁCE
BACHELOR'S THESIS

AUTOR PRÁCE JONÁŠ GLOSS
AUTHOR

VEDOUCÍ PRÁCE Ing. JINDŘICH MACH, Ph.D.
SUPERVISOR

BRNO 2012

Vysoké učení technické v Brně, Fakulta strojního inženýrství

Ústav fyzikálního inženýrství
Akademický rok: 2011/2012

ZADÁNÍ BAKALÁŘSKÉ PRÁCE

student(ka): Jonáš Gloss

který/která studuje v **bakalářském studijním programu**

obor: **Fyzikální inženýrství a nanotechnologie (3901R043)**

Ředitel ústavu Vám v souladu se zákonem č.111/1998 o vysokých školách a se Studijním a zkušebním řádem VUT v Brně určuje následující téma bakalářské práce:

Příprava a analýza nanostruktur v podmínkách UHV

v anglickém jazyce:

Preparation and analysis of nanostructures in UHV conditions

Stručná charakteristika problematiky úkolu:

Vrámci bakalářské práce bude provedena rešeršní studie v oblasti přípravy a analýzy 2D-0D nanostruktur v podmínkách UHV. Dále budou připraveny 2D - 0D nanostruktury (např. Au, Ga, nebo GaN) v ultravakuové aparatuře. Poté budou provedeny analýzy připravených nanostruktur metodou SPM, případně dalšími metodami.

Cíle bakalářské práce:

1. Proveďte rešerši v oblasti přípravy a analýzy 2D-0D nanostruktur v podmínkách UHV.
2. Připravte 2D - 0D nanostruktury (např. Au, Ga, nebo GaN) v ultravakuové aparatuře.
3. Proveďte analýzu připravených nanostruktur metodou SPM, případně dalšími metodami.

Seznam odborné literatury:

[1] Marius Grundmann, The Physics of Semiconductors, Springer-Verlag Berlin Heidelberg (2006), ISBN 3-540-25370-X.

Vedoucí bakalářské práce: Ing. Jindřich Mach, Ph.D.

Termín odevzdání bakalářské práce je stanoven časovým plánem akademického roku 2011/2012.

V Brně, dne 24.11.2011

L.S.

prof. RNDr. Tomáš Šikola, CSc. Ředitel ústavu	prof. RNDr. Miroslav Doupovec, CSc. Děkan fakulty

ABSTRAKT

Cílem této bakalářské práce bylo skoumání přípravy a analýzy nanostruktur v podmínkách vysokého vakua (VV). Teoretická část klade důraz na gallium nitridové (GaN) nanostruktury. Ty pak byly analyzovány rastrovacím tunelovacím mikroskopem (RTM). Aby bylo možné analyzovat připravené vzorky ve VV RTM, bylo provedeno elektrochemické leptání wolfrámového drátu. Tato práce zhrnuje postup k vytvoření wolfrámových hrotů pro RTM. Kapitola o výrobě wolfrámových hrotů zahrnuje popis princípu elektrochemického leptání. Obrázky vyleptaných hrotů byly provedeny pomocí rastrovacího elektronového mikroskopu. Zaostřování hrotů pak bylo vykonáno fokusovaným iontovým svazkem. V této práci je také představena metoda pro opětovné ostření RTM hrotů elektronovým svazkem, vykonávaná in-situ. Bylo dokázáno, že je možné rutinně obdržet wolfrámové hroty s poloměrem křivosti rádovo v nanometrech.

KLÍČOVÁ SLOVA

STM, SPM, Elektrochemické leptání, SEM, FIB, wolfrámové hroty, GaN, UHV, MBE

ABSTRACT

The purpose of this thesis was to study the preparation and analysis of nanostructures in Ultra High Vacuum (UHV) conditions. The theory section has a strong emphasis on Gallium Nitride (GaN) nanostructures. These were then analyzed by Scanning Tunneling Microscope (STM). In order to be able to analyze prepared samples in UHV STM, electrochemical etching of tungsten wire was carried out. This thesis gives an account on how to obtain tungsten tips for STM. The section dealing with tungsten tip fabrication includes description of electrochemical etching principle. Scanning Electron Microscope (SEM) images of etched tips and their further sharpening by Focused Ion Beam (FIB) was carried out. In this work a method for in-situ UHV STM tip revitalization by electron annealing is proposed. It was concluded that it is possible to routinely obtain tungsten tips with apex radius in the order of nanometers.

KEYWORDS

STM, SPM, Electrochemical etching, SEM, FIB, tungsten tips, GaN, UHV, MBE

Gloss, J. Příprava a analýza nanostruktur v podmínkách UHV. Brno: Vysoké učení technické v Brně, Fakulta strojního inženýrství, 2012. 41 s. Vedoucí bakalářské práce Ing. Jindřich Mach, Ph.D.

PROHLÁŠENÍ

Prohlašuji, že svou bakalářskou práci na téma "Příprava a analýza nanostruktur v podmínkách UHV" jsem vypracoval samostatně pod vedením vedoucího bakalářské práce a s použitím odborné literatury a dalších informačních zdrojů, které jsou všechny citovány v práci a uvedeny v seznamu literatury na konci práce.

Jako autor uvedené bakalářské práce dále prohlašuji, že v souvislosti s vytvořením této bakalářské práce jsem neporušil autorská práva třetích osob, zejména jsem nezasáhl nedovoleným způsobem do cizích autorských práv osobnostních a jsem si plně vědom následků porušení ustanovení § 11 a následujících autorského zákona č. 121/2000 Sb., včetně možných trestněprávních důsledků vyplývajících z ustanovení § 152 trestního zákona č. 140/1961 Sb.

V Brně dne ....

(podpis autora)

PODĚKOVÁNÍ

V první řade bych chtěl poděkovat vedoucímu práce, Ing. Machovi, Ph.D., za jeho rady při jejím vypracování. Poděkování patří také Ing. Nováčkovi, Ing. Neumanovi a Ing. Paverovi za jejich zájem o vysvětlování řešení problémů spojených s mou bakalářskou prací, ačkoliv byly jakkoliv triviální. Za korekturu angličtiny a důležité připomínky děkuji Ing. Kalouskovi, Ph.D, a panu De Mello. Taky bych rád poděkoval celému kruhu za jejich konstruktivní kritiku.
Největší díky patří samozřejmě mé rodině, která mi vytvořila zázemí a podporovala mě na cestě za dokončením této práce.

CONTENTS

1 **Introduction** 1

2 **Preparation of Nanostructures** 3
- 2.1 Thin Films . . . 3
- 2.2 Deposition of Thin Films by Low Energy Ions . . . 3
  - 2.2.1 LEI Interaction . . . 3
  - 2.2.2 Molecular Beam Epitaxy . . . 4
  - 2.2.3 Epitaxial Growth . . . 6
  - 2.2.4 LEI systems . . . 7
- 2.3 Preparation of GaN Thin Films . . . 10
  - 2.3.1 GaN and its applications . . . 10
  - 2.3.2 Methods for GaN deposition . . . 11

3 **Analysis of Nanostructures** 13
- 3.1 Scannning Tunneling Microscopy . . . 13
- 3.2 Atomic Force Microscopy . . . 14
- 3.3 STM Tip Fabrication and Treatment . . . 15
  - 3.3.1 Electrochemical Etching . . . 16
  - 3.3.2 SEM analysis . . . 17
  - 3.3.3 Sharpening by FIB . . . 17

4 **Experiments** 19
- 4.1 STM tips . . . 19
  - 4.1.1 Electrochemical etching . . . 19
  - 4.1.2 SEM images . . . 25
  - 4.1.3 FIB sharpening . . . 27
  - 4.1.4 UHV tip decontamination . . . 30
- 4.2 STM measurements . . . 33
  - 4.2.1 Etched and cut STM tips . . . 33
  - 4.2.2 Deposition of GaN and its analysis by STM . . . 35

5 **Conclusion** 37

References 39

1 INTRODUCTION

In this thesis is described in depth how to obtain sufficiently sharp tips for Scanning Tunneling Microscopy (STM) Ultra High Vacuum (UHV) analysis and their utilisation for examination of a Gallium Nitride (GaN) sample. The aim of this work was to prepare GaN nanostructures and then analyze them with Scanning Probe Microscopy (SPM) in UHV chamber. The characteristics of tips are crucial for the STM analysis. This led to a strong emphasis on STM tip preparation and treatment described in the experimental section of this thesis. The reason for GaN deposition was that it is the most widely used material for the manufacturing of nanostructures at the Institute of Physical Engineering in the Faculty of Mechanical Engineering, Brno University of Technology (IPE FME BUT).

In the year 1993 at the IPE the development of equipment necessary for deposition, modification and analysis of nanostructures in UHV began. David Škoda's work from 2001 [34] dealt with the SPM and a part of his work was connected to the STM tip fabrication. The deposition of GaN in the IPE UHV chambers was recently described by Jindřich Mach in [19, 20].

The theoretical section of this thesis firstly deals with the background to deposition of nanostructures (namely thin films) in general. This chapter provides description of Low Energy Ion (LEI) interactions with the surface and a most commonly used method for GaN deposition at IPE - Molecular Beam Epitaxy. The chapter is then concluded with LEI systems and their application for GaN deposition at IPE.

The next chapter briefly reports on the theory behind the analysis of nanostructures with SPM and is terminated with a section on STM tip fabrication. The last one includes a research in the area of tip fabrication, which is then concluded with a description of a method which will be used for manufacturing of STM tips. Scanning Electron Microscopy (SEM) is then mentioned as a tool for quantitative description of created STM tips. A brief explanation to Focused Ion Beam (FIB) concludes the theoretical section since it was used for sharpening of the tips.

The practical part of this thesis brings results of tip fabrication alongside with its SEM images. The sharpening of the tips by FIB is analyzed in the following subsection and the section on STM tip fabrication ends with a proposed method for in-situ tungsten STM tip decontamination from its native oxides. It then follows that a section on GaN deposition with its STM analysis for which both etched and cut STM tips were used. All of the results are discussed in the experimental section.

2 PREPARATION OF NANOSTRUCTURES

2.1 Thin Films

Thin films are defined to be three dimensional structures, which have quantum effects occuring in one dimension. The outcomes in the other two are considered classical. These are most commonly used in electronic semiconductor devices. The reason for the quantum effects is that the atoms are constrained in one dimension and can only move, i.e. interact in the plane. Thin films are therefore often referred to as two dimensional structures. Development of Scanning Probe Microscopy (SPM - see chapter 3) allowed investigations on an atomic scale. This has increased the interest in thin film creation and manipulation, thus exploring further possibilities.

The main focus of this section is on the creation of thin films, but as it will be mentioned further on, in the process of their growing one dimensional and zero dimensional structures grow up. Through thin films were discussed 2D to 0D nanostructures. Furthermore, GaN thin films are the main material investigated at IPE FME BUT and it is therefore reasonable to do a research study in this field.

2.2 Deposition of Thin Films by Low Energy Ions

2.2.1 LEI Interaction

Low energy ions (LEI) are defined to be atoms with charge, which energy is below 100 eV. Because of this energy, the main action that takes place is the collision of the ion with the substrate. The main attributes that affect the result of this collision are structure of the substrate, its temperature and characteristics of the ion - its mass, charge and energy [24]. The results of ion collision are shown in Figure 2.1. The ion collides with surface of the substrate and can be either reflected or absorbed. These two main features then split into different interactions. Each interaction can be succeeded by foton or electron emission, through which the surface atoms go back to its stable states.

Neutralisation and Scattering If a substrate, which the ion is colliding with is conductive, charge exchange takes place between the ion and the substrate. This charge is then dispersed in the conductor. Materials used for ion deposition therefore have to be conductive, so that they will not charge and hence change its electronic properties and repel incoming ions. Charge transmission can take place even when the ion is approaching the wall [12]. If the ion is neutralised, it can scatter from the surface.

Penetration and Sputtering If the ion is neutralised and it is not directly scattered, these two actions can take place. Sputtering occurs when the ion has sufficient energy to break the chemical bonds that link the target atoms and even give them excessive kinetic energy to leave the surface. This is one of the irradiation effects of ion deposition. Further references to ion irridation will be discussed in detail

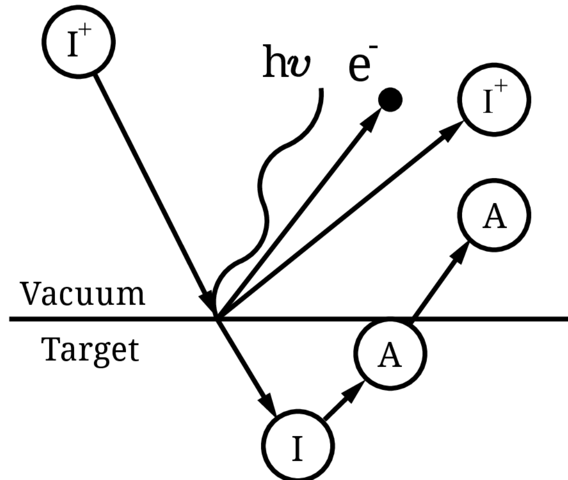

Figure 2.1: Main results of ion-substrate collisions.

when describing GaN thin film creation on page 10 in section 2.3 by low energy ion deposition. The incident ion when neutralised, becomes an atom and could be then either adsorbed or scattered. For both surface penetration and sputtering a treshold energy has to be acquired by incident ions and hence these effects can be suppressed by a well defined ion energy.

Adsorbtion Adsorbtion takes place, when the ion becomes part of the surface, or penetrates further into the solid. A distinction in definitions of absorbtion and adsorbtion is that absorbtion deals with the whole volume (i.e. fluid and solid), whereas adsorbtion deals only with the surface. However, low energy ions do not have sufficient energy to penetrate too deep [21].

2.2.2 Molecular Beam Epitaxy

Molecular beam epitaxy (MBE) is a technique for epitaxial growth via the interaction of one or several molecular or atomic beams that occurs on a surface of a heated crystalline substrate. It is used for preparation of various semiconductors. In order for the molecules to get to the substrate, their mean free path λ has to be larger than the distance the atoms travel. To achieve this, the pressure in the chamber has to be in the order of 10^{-8} Pa. Considering the sticking coefficients of different molecules, the pressure condition can be generalised to UHV. This pressure satisfies the demand for the growth of a clean epilayer, even though the deposition rate is below 1000 nm per hour. This feature of MBE allows the films to grow epitaxially on the substrate. A number of different ion or atom emitting cells can be deployed to modify the surface of the target. Figure 2.2 shows the basic principle with effusion cells, which are most commonly used for thin film deposition.

In systems where the substrate needs to be cooled, the UHV environment within the growth chamber is maintained by a system of cryopumps, and cryopanels, chilled using liquid nitrogen or cold nitrogen gas to a temperature close to 77 K, as shown in Figure 2.2. Cryogenic temperatures act as a sink for impurities in the vacuum.

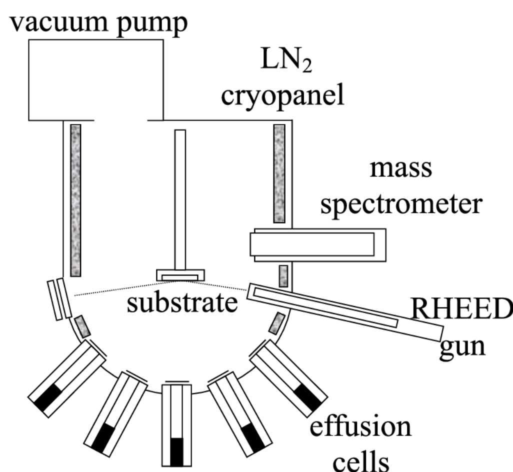

Figure 2.2: Cell for Molecular Beam Epitaxy[27]

Therefore the vacuum level of the cell has to be several orders of magnitude higher to deposit films under these conditions. In other systems, the wafers on which the crystals are grown may be mounted on a rotating platter which can be heated to several hundred degrees Celsius during operation [27].

The MBE began as the "three-temperature method" developed by K.G. Günther in 1958 [10]. In 1960s was this technique used for growing of stoichiometric, polly-crystalline films on glass substrate. In the 1970s epitaxial growth of monocrystalline GaAs was achieved on clean single-crystal substrates under improved vacuum conditions and the chemical processes involved in the MBE were studied by J. R. Arthur [3] and C.T. Foxon et al [9]. The next decade brought introduction of gas sources and observations of oscillations in intensity of features in the Reflection High Energy Electron Diffraction (RHEED) patterns. It followed that two more improvements (i) pulsed mode of supplying the reactatnt species to the growing epitaxial layer assisted by Ultra Violet (UV) light or ionized hydrogen and (ii) the UHV multi-chamber system combining Focused Ion Beam (FIB) and etching operation together with MBE growth and characterisation equipment. The 1980s thus made it possible for the production of complex device structures.

Since the 1990s, MBE has been used for the construction of 2D to 0D quantum structures, also called Low Dimensional Heterostructures. MBE made possible the fabrication of heterostructures with its composition varying on spatial scale of one to one hundred crystal-lattice constants. These have distinctive physical properties resulting from the occurence of an intermediate size between two physical domains. Firstly it is microscale - quantum effects domain of lattice constants or the de Broghlie wavelength λ_c of the charge carriers. The second is the macroscale domain associated with quasi-classical motion of the charge carriers. The motion of carriers in a direction where potential barriers created by heterointerfaces confine them to an area that has a size belonging to the microscale, is strongly quantized, while the carriers motion in the directions where no such confining barriers exist, is quasi-classical [18].

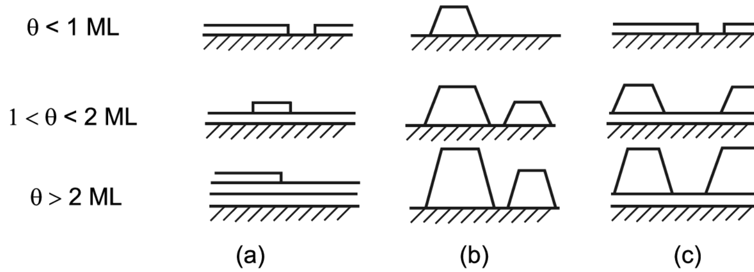

Figure 2.3: Schematical presentation of three growth models as a function of Φ monolayer coverage (ML) (a) layer on layer (b) islandes (c) layer and islands[19]

According to [18], the MBE deposition induces these effects on the surface of the target:

1. adsorbtion of the atoms or molecules of the incident beam
2. surface migration and dissociation of the adsorbed molecules
3. incorporation of the constituent atoms into the crystal lattice, i.e. intersticial atoms
4. thermal desorption of the species not incorporated into the crystal lattice, i.e. sputtering

These have been previously discussed in 2.2.1, page 3.

2.2.3 Epitaxial Growth

Epitaxial growth refers to deposition of crystalline overlayer on a crystalline substrate, when the overlayer structure is strongly affected by the structure of the substrate. Therefore, they have identical crystal structure. Epitaxial thin films could be grown on a substrate of the same material, in which case it is homoepitaxial growth, or on a different material, which is called heteroepitaxial growth. The growth can be divided into three fundamental modes. The first one is called Frank-van der Merver. In this mode the bond between the substrate and incident atoms is stronger than the adherence between deposited atoms. This type of growth is shown schematically in Figure 2.3 (a), where Φ pictures the quantity of the material required to cover one complete atomic layer. In a different scenario when deposited atoms are more attracted to each other than to substrate atoms, growth of islands takes place. This growth mode is pictured in Figure 2.3 (b) and is called Vomer-Weber growth. In case that the attractive forces are equal, third type of layer creation takes place. This one (Figure 2.3 (c)) is a combination of the two previous ones and it is called Stranski-Krastanov growth mode [19].

Epitaxially grown thin films are important in, for example, the production of semiconducting electrical equipment, magnetic recording media (multilayers) and magnetic reading heads. Presently, the epitaxial growth is used in preparation of artificial single crystals, since the semiconducting devices (transistors and thus computers) are critically dependent on the availability of very perfect and extremely pure semiconductor crystals [2].

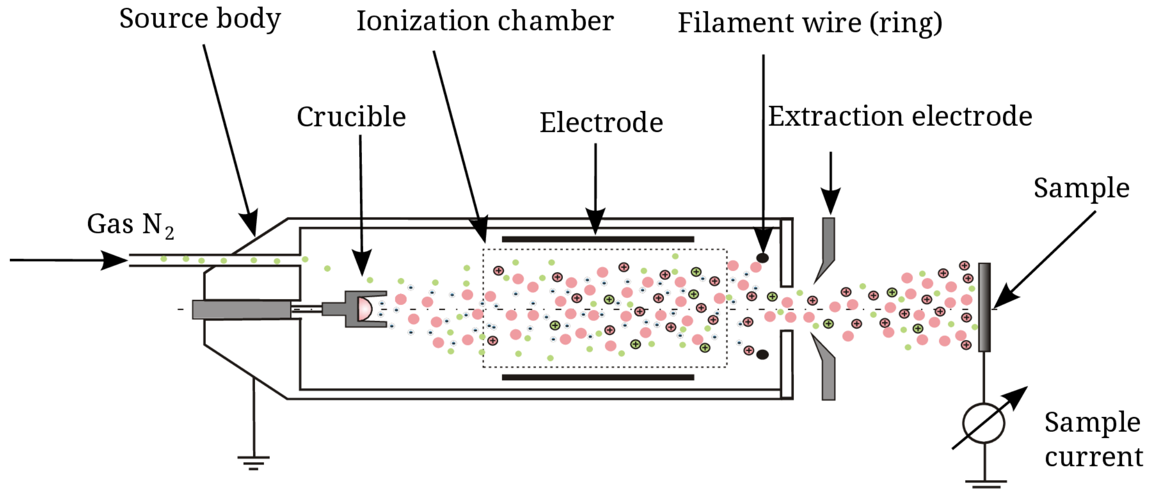

Figure 2.4: Schematic view of ion-atomic beam source commonly used for Gallium Nitride deposition at IPE

2.2.4 LEI systems

This subsection gives a quick overview over the thin film deposition systems, that are most commonly used when working with GaN. Such systems have to fulfill very specific requirements. This section will focus on thin films created by MBE. However, any of the mentioned devices could be used for other methods that are working not with single layer of atoms, but with layer thickness in the order of nanometers. The application of MBE requires excellent film uniformity and reproducibility of growth conditions. The reason for this is that for example the uniformity in thickness and composition depends on the uniformity of the molecular beams. This uniformity depends on the geometry of the source-substrate system (see Figure 2.2), and on the angular flux distribution. Sufficiently large source to substrate spacing and isotropic flux distribution in the solid angle subtended by the substrate fulfills this. Reproducibility of growth conditions depends on the long term stability.

A very important factor that influences the MBE process is the structure of the molecular species used for the MBE growth. This results from the differences in the surface chemistry of the growth process relevant to different molecular species of the same element. For example, the dissociation mechanisms of two arsenic species, dimeric (As_2) and tetrameric (As_4) are quite different during the MBE growth of GaAs and related III-V compounds [18].

Ion-Atomic Beam Sources The ion-atomic beam source designed in the IPE laboratory produces a mixture of atoms and ions and, hence, combines an effusion cell generating beams of thermal atoms (energy of $0.1 - 1.0$ eV) and an electron-impact-ion beam source. This source generates low energy ion beams in the energy range from 30 eV to 200 eV. A schematic of the source is shown in Fig. 2.4.

Electrons having initial thermal energies are emitted from a heated tungsten filament and accelerated by a voltage of ~ 100 V towards a grid forming walls of a cylindrical ionization chamber (an envelope of an ionizer), and consequently enter

the ionization area. The stainless steel grid defines both a constant potential inside the ionization chamber and an acceleration voltage between the cathode filament being at a floating potential and the grid. In this way electrons can collide with neutral atoms inside the ionization chamber at a well defined energy optimized to the most effective ionization (i.e., the highest ionization cross section). For most of inert gases this energy is close to 100 eV [29]. Additionally, the potential of the ionization chamber defines the energy of ions at the earthed target (ion energy at the target is defined by the potential difference between the place of ion creation and the target). This fact together with the floating potential of the filament makes it possible to change the target ion beam energy while keeping the electron energy close to 100 eV and, hence, to the most effective ionization conditions.

Effusion Cell Other electrons not interacting with atoms go through the grids of the ionization chamber and are post-accelerated towards the crucible being at the typical potential $U_c = 1000$ V. In this way the crucible is heated by electron bombardment to a temperature sufficient for the evaporation of a material inside the crucible. Crucible does not have capacity for large amounts of the material. Therefore, if the effusion cell is used for deposition over large areas (e. g. industry), instead of a crucible can be placed the evaporated material in a rod form. A rod form saves the effort of opening the chamber in order to exchange the crucible (or to fill it), but increases demands on construction. The evaporated atoms with thermal energy pass through the grid of the ionization chamber by an effusion flow along straight trajectories towards the target [20]. Materials that are most often deposited using the effusion cell are Ga, Au, Si, Fe, Ag [19]. Atoms in the effusion cell cannot be focused by electro-magnetic field. One of possible solutions is to use collimator. It is a rod that is separated into small apertures to achieve broad and uniform beam of atoms. It is hence used for large samples and considering the wavelenghts of the atoms and the width of apertures, interference has to be taken into account. Other way how to focus the thermal atoms created in the effusion cell is to apply a miniature Laval nozzle as the first gap of the source, which would lead to creation of supresonic atom beam. The goemetry is very important, since the atom beam is focused only through the shape of the particular apertures. Figure 2.5 shows the Laval nozzle, which creates supersonic beam and the sonic nozzle (or, a Venturi tube), which increases the speed of the atoms below supersonic speed.

The gas is introduced into the source through an UHV valve, the pressure in the main chamber is commonly $p \sim 10^{-5}$ to 10^{-6} Pa. Ionized gas atoms together with the atoms evaporated from a crucible form the major constituents of the beam. The positive ions generated in the ionization chamber are pulled out by an extraction electrode. During operation RHEED is often used for monitoring the growth of the crystal layers. A computer controls shutters in front of each furnace, allowing precise control of the thickness of each layer, down to a single layer of atoms [20]. Intricate structures of layers of different materials may be fabricated this way. Such control has allowed the development of structures where the electrons can be confined in space, giving quantum wells or even quantum dots. Such layers are now a critical part of many modern semiconductor devices, including semiconductor lasers and light-emitting diodes [27].

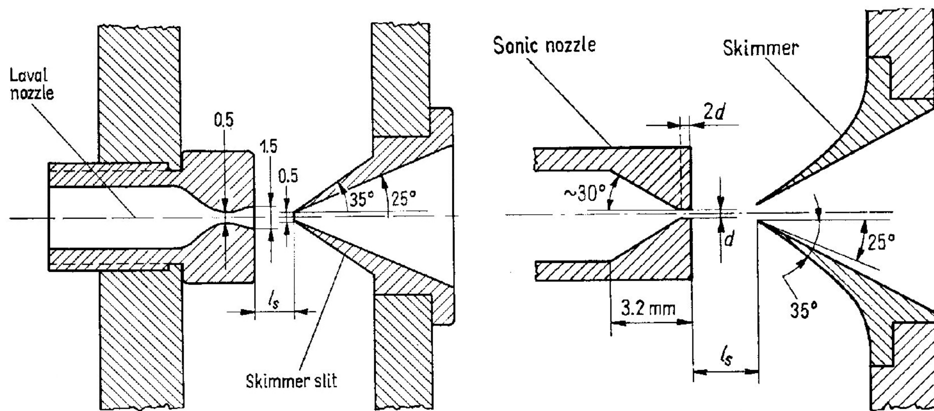

Figure 2.5: supersonic

In order to define exact dimensions in technical drawings, trajectories of electrons and ions (e.g. N_2^+ with $E_k \sim 100$ eV) inside the ion-atomic beam source could be simulated by the EOD simulation program[17] being at a negative potential towards the earth. Additionally, the negative potential at the extraction electrode influences the profile of the ion beam [20].

Focused Ion Beam Technology (FIB) servers to sputter the atoms off the target surface or to scan the object in order to acquire a picture. This technique utilises, as is written in its name, charged atoms. The reason for this is that the ions have larger mass and energy and hence they do not penetrate underneath the surface of the target and all of their energy is dispersed in the collision. When the energy is appropriate, this results in sputtering and it was the reason why this technique was deployed in order to further sharpen the electrochemically etched tips for Scanning Tunneling Microscopy.

2.3 Preparation of GaN Thin Films

After the general introduction to MBE and LEI systems, let us focus on the research done in this area at IPE. As was mentioned in the introduction, the development began in the 1990s. Since then was completed and over the years improved apparatus shown in figure 2.6

2.3.1 GaN and its applications

GaN forms a basis of system of semiconductors with potential use in electrical industry due to its wide band gap (and thus a large breakdown voltage), hardness, high thermal (up to 1000 °C) and chemical stability and high electron saturation velocity. These characteristics allow the material to be used at elevated temperatures and in environments where the properties of other semiconductor systems would degrade. GaN has a wide range of applications, for instance in light emitting devices operating in the blue- and ultraviolet (UV) spectral regions and in solar cells. The reason for this are the direct tunable band gaps (it is a III-V semiconductor) of this material providing a wide spectral range, including the visible and ultraviolet. Its characteristics combined make GaN a very promising material for high power, high frequency applications where traditional Si and SiGe technologies fail. Laser diodes on GaN base are used in Blue-ray technology for data reading. Hardness of GaN allows to use it as a protective layer, its high thermal stability [19].

In the 1960's and 1970's, researchers were unable to produce nitride materials (particularly GaN) of high quality. They were facing problems with lack of suitable lattice-matched or thermally matched substrate, inability to obtain p-type doped

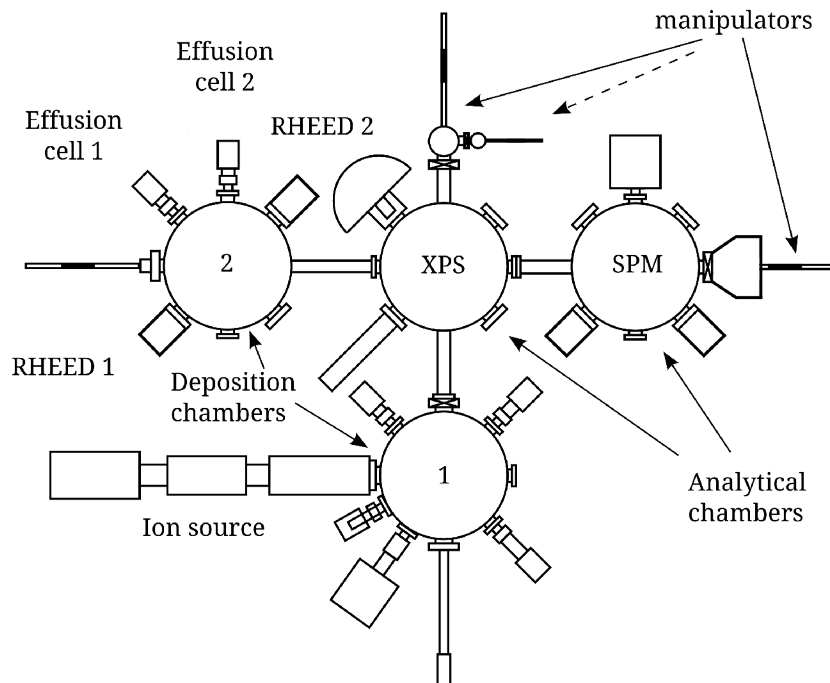

Figure 2.6: UHV chambers for deposition and analysis of thin films

material etc. The course has changed with the use of MBE as a thin film and crystal growth technique in the 1990s. Since then, the knowledge of basic properties of GaN has been greatly increased. Table 2.1 shows some of the most important properties.

Table 2.1: Some of the GaN characteristics

Band gap energy	$E_g(300K) = 3.39$ eV
	$E_g(1.6K) = 3.50$ eV
Thermal conductivity	$\kappa = 1.3$ W cm^{-1} K
Monolayer thickness	2.59Å
Ga site (atomic) density	$N_{Ga} = 4.28 \times 10^{22}$ cm^{-3}
Ga surface density	$N_{Ga} = 1.1 \times 10^{15}$ cm^{-2}

The negatives GaN faces as a semiconductor is the lack of GaN substrates, on which it can grow epitaxially, since no substrate is able to match it physically and thermally. The most commonly used substrates are Si, GaAs, SiC, Al_2O_3 with various crystalline orientation of the wafer. In the lab of IPE, the substrate commonly used for 2D to 0D nanostructures are Si wafers. These are grown from crystal having a regular crystal structure, with silicon having a diamond cubic structure with a lattice spacing of 5.43 Å. When cut into wafers, the surface is aligned in one of several relative directions known as crystal orientations. Preferential growth is defined by the Miller index with [100] (cubic form of GaN) or [111] (mostly wurtzite form) faces being the most common for silicon as a substrate [7, 26]. The reason for the use of Si is that it is the most widely used material in microelectronics and exploration of GaN-Si properties would lead to Light Emmiting Diode and laser integration. Usually grows a GaN layer of 30 nm before the MBE deposition [19].

2.3.2 Methods for GaN deposition

Deposition of GaN nanostructures is currently done using a wide variety of methods. The technical principles of some of them used in our laboratory were described in 2.2.4. From the point of view of the binding properties (i.e. reactions with the surface) of GaN, the methods can be divided into chemical and physical.

Chemical methods are commonly known as Chemical Vapour Deposition (CVD). Metalorganic Chemical Vapour Deposition (MOCVD) in other words Metalorganic Vapour Phase Epitaxy (MOVPE) and Hydride Vapour Phase Epitaxy (HVPE) belong to this group. MOCVD is the most common method used in industry, where the reservoir of Gallium is Trimethylgallium ($Ga(CH_3)_3$), which reacts with amonnia NH_3. Method HVPE uses the reaction of Hydrogen Chloride (HCl) and liquid Ga, thus creating Gallium Chloride (GaCl). GaCl reacts with NH_3 and creates the desired compound. To improve the layer grown by these methods the Epitaxial Lateral Overgrowth (ELO) modification is used. In ELO is utilised a dielectric mask, which preserves the selective epitaxial growth in uncovered parts of the substrate. When

the height of the grown layer is sufficiently high, by change in deposition conditions is achieved preferential lateral growth which serves as a catalyst for connection of separated parts into a cohesive film. Similar modification is pendeoepitaxy, when the column crystallized GaN structures are covered by a dielectric mask. Here lateral and vertical growth takes place until all of the separated parts eventually form a column.

Physical methods are represented by Physical Vapour Deposition (PVD). The most important method is MBE, see section 2.2.2, page 4. In the case of GaN deposition, Ga atomic beam with thermal energy only targets the substrate alongside with either Nitride atomic source or ions of either Ammonium or Nitrogenium. Should any nanostructures be prepared, it would be by the Ion-Atomic Beam Source (its function is described in section 2.2.2,on page 7), which would emit a beam of Ga atoms and N_2^+ ions.

3 ANALYSIS OF NANOSTRUCTURES

Technological and theoretical developments in the beginning of 20th century opened way for miniturisation, ranging from electronical equipment to mechanical parts, as Richard Feynmann predicted in his talk “There’s Plenty of Room at the Bottom” at Caltech in 1959:

> But I am not afraid to consider the final question as to whether, ultimately - in the great future - we can arrange the atoms the way we want; the very atoms, all the way down!

Microscopes with increasingly higher resolution were thus required in order to analyse new concepts and even to create structures with atomic resolution. In this chapter was widely used [34]

3.1 Scannning Tunneling Microscopy

In 1981 was firstly demonstrated Scanning Tunneling Microscope (STM) by R. Binnig and H. Rohrer [4]. The basic principle of STM is measuring the relative distance between the surface of the sample and the scanner during the scanning process in the order of tens of picometers, achieving atomic resolution. The very characteristic feature of STM is therefore the need for sample’s conductivity. STM is based on the principle of tunneling current flow between the sond and the sample (amplitude is defined by equation 3.1), even though the energy of the particle E is smaller than the height of the barrier V_B. The sond consists of a conductive material with a very sharp apex ideally terminated with a few atoms. Tunneling is a quantum effect, which assigns a particle probability to overcome a potential barier of defined energy. This barrier can be modified by various means of which are used at IPE the sample-to-tip distance and the potential difference.

The tunneling current of electrons i_t is:

$$i_t = i_0 \exp\left(-\sqrt{8m_e\left(V_B - E\right)/h^2}d\right) \tag{3.1}$$

where e is the elementary charge, m_e mass of the electron, d width of the barrier and h is Planck’s constant [22].

Considering the amplitude of metal work function (4-5 eV) and the constants, $-\sqrt{8m_e\left(V_B - E\right)/h^2} \approx 1\text{Å}^{-1}$. Change in width of potential barrier by 1 Åwould therefore cause decrease in tunneling current by one order. This gives the STM an opportunity to measure very small (picometric in terms of distance) changes of the width of the barrier. Also, most of the tunneling current flows through closest atoms of the apex (the impact of the rest is negligible) and therefore it is desirable to have one atom on the very end of the tip. Apart from sharpness of the tip are important the piezo manipulators and restriction of vibrations. All of these issues were addressed in the experimental part of this thesis, in section 3.1, page 13.

STM is also used for measurement of volt-ampere characteristics of the sample surface. This method is called Scanning Tunneling Spectroscopy (STS). The feedback loop which adjusts the height of the tip above the sample is set off and current amplitude dependant upon the variable potential is measured. From revealed relations it is possible to gain information about the electrical conductivity, work function of the electrons in the sample (or Fermi energy E_F) and the electron band structure. STS also serves for measurement of relations between current and the tip-to-sample distance with potential held constant.

3.2 Atomic Force Microscopy

A few years after the invention of STM, Atomic Force Microscopy (AFM) was introduced in the 1986 by the same team under R. Binnig and H. Rohrer. AFM studies the surface of the sample by measuring mutual force interactions between atoms of the very sharp apex and the sample surface atoms, which does not have to be conductive compared to STM. Forces that are measured in AFM include mechanical contact force, chemical bonding, electrostatic forces, magnetic forces etc. However, should the scanned sample be conductive, it is possible to measure the current flow and combine the advantages of STM and AFM into Conducting AFM (CAFM)[16]. One of the modes is a constant height mode, when through the deflection of the cantilever the force is measured. However, if the tip was scanned at a constant height, a risk would exist that the tip collides with the surface, causing damage. Hence, a feedback mechanism is employed to adjust the tip-to-sample distance to maintain a constant force between the tip and the sample.

Similarly as was the case of STM, piezoelectric crystals are used for the navigation of the tip on the sample, when either the tip and/or the sample is moved. The resulting map of the area $z = f(x, y)$ represents the topography of the sample. The AFM can be operated in a number of modes, depending on the application. In general, possible imaging modes are divided into static (also called contact) modes and a variety of dynamic (non-contact or "tapping") modes where the cantilever is vibrated at a measured frequency.

Cantilever is the part of the AFM that is in direct contact with the surface. Cantilever arm is usually of A letter shape and is integrated into a rectangular girder. When using optical method for arm displacement detection is the top of the arm covered by reflecting layer. A cantilever is defined through its dimensions s, t, v [μm], spring constant k [Nm^{-1}] and resonant frequency f_0. The tip is either of conical or pyramidial shape and together with the cantilever it is typically made of highly doped silicon to avoid charging and allow combination of tunneling and force microscopy experiments[22]. Important parameters of the tip are its apex radius and the top angle. AFM cantilever is also used at IPE, but the technique for its preparation will not be included, because it is much more difficult [32]. Most cantilevers are produced through microfabrication process in the semiconductor industry [22].

At the IPE is used Omicron SPM UHV head shown and described in figure 3.2. This SPM offers utilisation of both STM and AFM in one instrument. *IMPROVE*

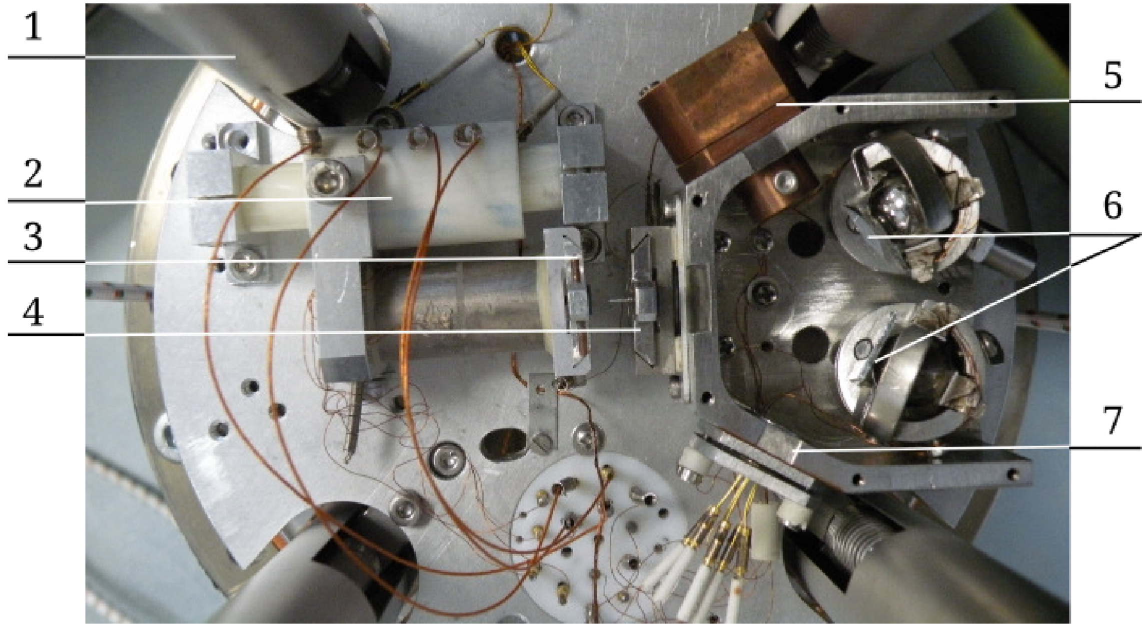

Figure 3.1: Omicron SPM UHV head used at IPE. The most important elements include 1) dumping, 2) piezoelectric inchworm, 3) sample holder, 4) STM tip holder (in figure) or AFM cantilever holder, 5) LED, 6) mirrors with piezoelectric motors, 7) photodetector

3.3 STM Tip Fabrication and Treatment

Desired properties for the STM are defined very clearly by the need of highest possible resolution. While it is dependant upon interconnected physical and technical features of the apparatus, the apex shape is of the key parameters of the whole system, alongside with the shape of the whole tip.

Slim and long tip gives more precise information about the investigated profile because of deeper penetration. On the other side, thick apex would be more resistant against underirable oscillations. Exponential apex shape seems to be the best solution to this [13, 31, 28]. After the invention of STM, many ways [14] of tip preparation for both in situ UHV analysis and analysis at room conditions were developed.

The most established methods have become electrochemical etching and cutting of metallic wire. Cutting 3.2, after acquiring some experience, is the quickest way how to obtain sharp tips and is used for example in the Nanosurf Easyscan 2 STM [23] commercial microscopy. Cut tips are usually of Platinum (75%) Irridium (25%) (Pt/Ir). However, although this method quickly provides relatively sharp tips, they are not reproducible, which does not affiliate with methods of science. Moreover, cut tips might have several minitips, of which the one closest to the surface gives the information about the surface conductivity. If there are several tips, the tip from which electrons tunnel might change when the tip is scanned. This gives double or even multiple imaging of features at the surface.

The size, shape and cleanliness of a STM tip are very important for the resolution

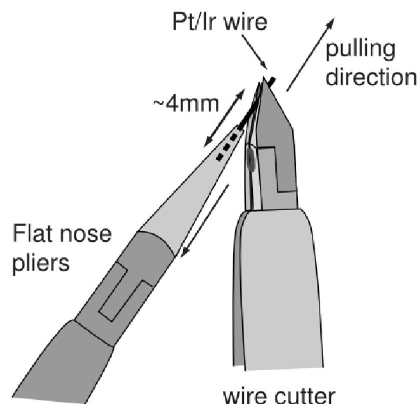

Figure 3.2: Schematic view of Pt/Ir wire cutting [23]

of a STM. If the tip is not free of contamination and oxide, the tunnel junction may be unstable and cause irregularities in STM imaging. The tip therefore has to be prepared carefully. For UHV, tungsten tips are frequently used. A tungsten tip has to be prepared by electrochemical etching, because of the hardness of the material [8].

3.3.1 Electrochemical Etching

This thesis will focus on electrochemical etching as a particular part of STM tip preparation. Etching takes place either naturally (chemical etching), since chemical reaction takes place between the wire and the electrolyte, or electrochemically, due to potential difference between electrodes. Natural reaction is not desirable because when the tip would be etched off to lowest apex radius and taken out of the solution, the electrolyte would still interact with it. This would result in blunt tips. Sharpest tips would therefore be obtained by electrochemical etching. Electrical field will be created between two electrodes - etched wire and an electrode in the electrolyte. When the tip would have desired properties, the etching process could easily be halted by setting the potential difference off. The aim of this thesis is to analyze samples in UHV and for this is the best material tungsten [14]. For this reason the STM tips for UHV will be fabricated from this substance.

Equation 3.2 gives an overview of the electrochemical reaction that takes place in the meniscus created by the wire immersed in KOH.

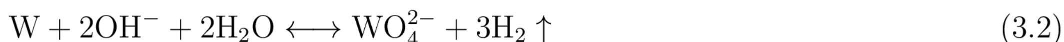

$$W + 2OH^- + 2H_2O \longleftrightarrow WO_4^{2-} + 3H_2 \uparrow \qquad (3.2)$$

Anodic process is oxidation of tungsten and cathodic reaction is depolarisation of OH^-. In water is anion WO_4^{2-} dissolved and $H_2WO_5{\cdot}H_2O$ formed. Figure 3.3 shows the creation of meniscus around the tungsten wire (left) and the effect of the etching procedure of the wire.

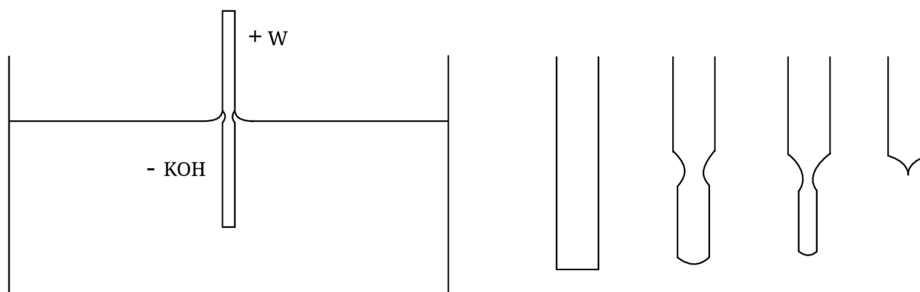

Figure 3.3: Left: Schematic view of the meniscus created by wire dipped in KOH. Right: Etching process

3.3.2 SEM analysis

Scanning Electron Microscope (SEM) was invented by Manfred von Ardenne in 1937. It is used to image a sample by scanning it with a beam of electrons in a raster scan pattern. The beam of electrons emmitted from tungsten filament is accelerated by the filament-sample potential (0.1 keV to 30.0 keV) difference and focused by electromagnets (beam width of $\sim 10^1$nm). The electrons interact with the atoms that make up the sample producing signals that contain information about the sample's surface topography, composition, and other properties such as electrical conductivity [25].

3.3.3 Sharpening by FIB

The Focused Ion Beam (FIB) system uses an ion beam to raster over the surface of a sample in a similar way as the electron beam in a SEM. The generated secondary electrons (or ions) are collected to form an image of the surface of the sample. The ion beam allows the milling of small holes in the sample at well localized sites, so that cross-sectional images of the structure can be obtained or that modifications in the structures can be made. Most instruments combine nowadays a SEM and FIB column. Generally the ion beam will be used for milling and the electron beam for imaging. It allows non-destructive imaging at higher magnifications and with better image resolution, and also more accurate control of the progress of the milling [15].

4 EXPERIMENTS

This chapter will acknowledge the reader with changes and improvements of the equipment in the laboratory at IPE FME BUT and how was the aim of this bachelor thesis met. Main focus is on the preparation of extremly sharp tungsten tips for STM, made by electrochemical etching and acuminated by FIB. In this section is also mentioned the in-situ revitalisation of tungsten tips by focused electron beam.

Second part of this chapter deals with a comparison of cut and etched tips. For this was carried out STM topography measurement of Highly Ordered Pyrolytic Graphite (HOPG) at room conditions for both kinds of tips. After this follows a GaN deposition concluded with STM analysis of the prepared sample.

4.1 STM tips

4.1.1 Electrochemical etching

According to section 3.1, page 13, the STM tips have to fulfill a long list of requirements and their production involves many variables. Table 4.1 gives a full list of those considered for electrochemical etching. Some of the variables have been

Table 4.1: Variables in electrochemical etching

Variable	Static
Potential	6-12V
Dip depth	~3 mm
Wire width and type	300 μm tungsten wire
Type and concentration of electrolyte	2 M KOH
Vibrations	uncontrolable
Current flow	DC

held constant according to sources [8, 33] as being the best parameters. The DC voltage method was chosen, because, according to [5], making tungsten tips with AC method without another refining technique is known to result in fairly blunt tips. The apparatus for static electrochemical etching, whose main body is shown in figure 4.3, was previously used at IPE and its function was described in [34]. Figure 4.1 shows the improved experimental setup.

At the heart of the setup were the electrodes. Tungsten wire as the anode and a circle of stainless steel around it as a cathode. Both of them were immersed in an electrolyte, Potassium hydroxide (KOH). The electrolyte created around the wire a meniscus, shown in figure 4.4 on right side (4). Before each etching process has begun, the stainless steel ring (2) was centered around the wire. This was done in order to apply symmetrical electric field to every point of the wire. The wire (3) was supposed to be kept perpendicular to the KOH surface. A micrometer screw gauge (figure 4.4 left) was used to adjust the dip depth of the wire.

The anode and the cathode were then brought into an amplifying circuit. Figure 4.2 describes the circuit for amplification of potential output from LABview®designed and built with the help of Ing. Zdeněk Nováček. The need for amplification arised

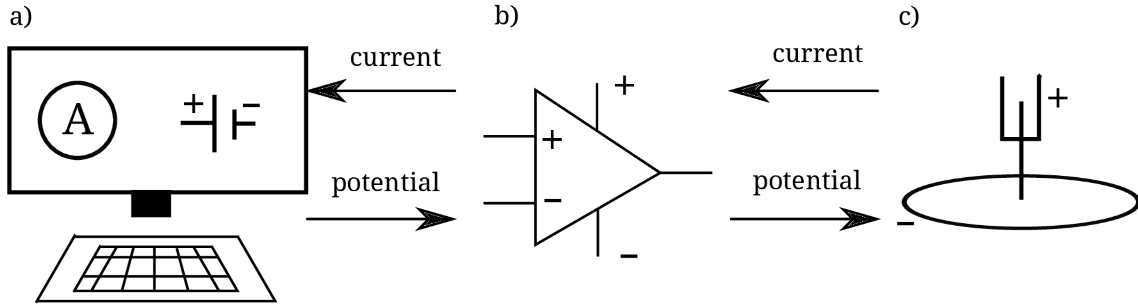

Figure 4.1: Schematic view of the experimental setup for electrochemical etching. a) represents a computer with a DAQ card, which sets potential and reads current, b) is the amplyfing circuit shown in figure 4.2 and c) is the electrochemical etching setup from figure 4.3.

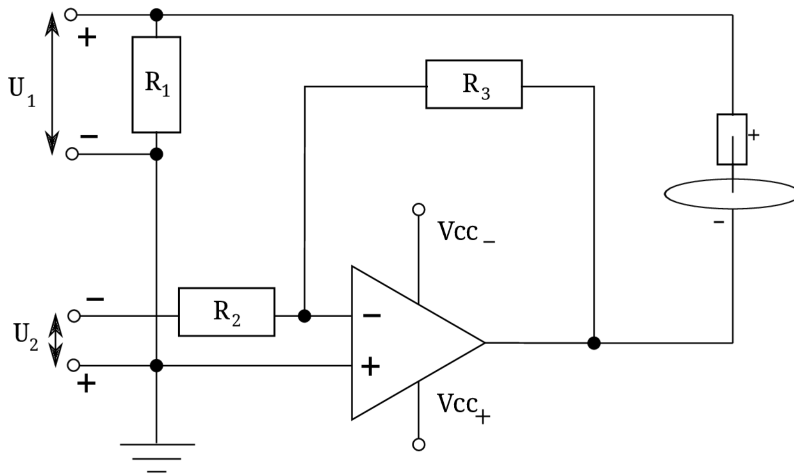

Figure 4.2: Schematic view of the circuit employed in figure 4.1 in order to magnify the potential output of the PC card. U_1 represents the potential measured in order to acquire current flow. U_2 is the potential output from the PC card. $Vcc_{\pm}$ is the amplifying potential of 15 V. The resistors are $R_1 = 250\,\Omega$, $R_2 = 1\,\text{k}\Omega$, $R_3 = 500\,\Omega$.

from the fact that dependencies of 6 V to 12 V were to be measured, but the card was only able to supply ~ 10 V.

The amplification circuit consisted of an output potential $U_1 = U(t)$ and an input potential $U_2 = 0 - 6$ V. The output potential was extracted from the current flow in the circuit through the load $R_1 = 250\,\Omega$. Resistor $R_2 = 1\,\text{k}\Omega$ served as a load lowering the potential on the amplifier. Amplifier (e.g. TL071) was supplied by an external source of 15 V. The load $R_3 = 500\,\Omega$ served as a back-loop for the amplifier. Finally, the voltage was applied to the etching setup.

In the last step, a software interface has been created by Ing. Michal Pavera for simple operation of voltage output and saving of current-time relations. It can be argued that this could have been done with a data-collecting oscilloscope, without taking too much trouble of creating the hardware and software grid. However, it was the process shut off control switch, which was the main advantage of the setup. Shut off control switch has prohibited further etching when the tip has fallen off.

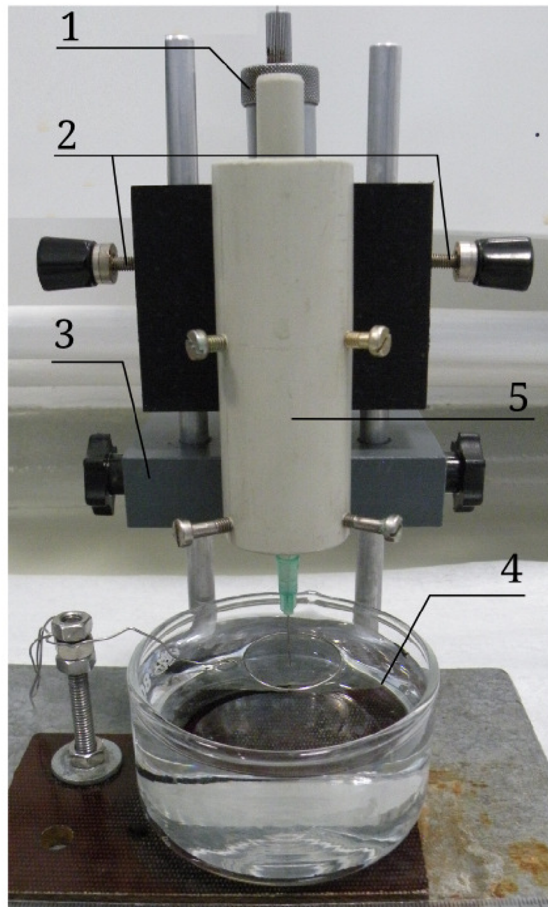

Figure 4.3: The main body of the apparatus for static electrochemical etching. (1) micrometer screw gauge (detail in figure 4.4), (2) securing screws, (3) main holder, (4) KOH electrolyte in a glass beaker (detail in figure 4.4), (5) tubus supporting the tungsten wire.

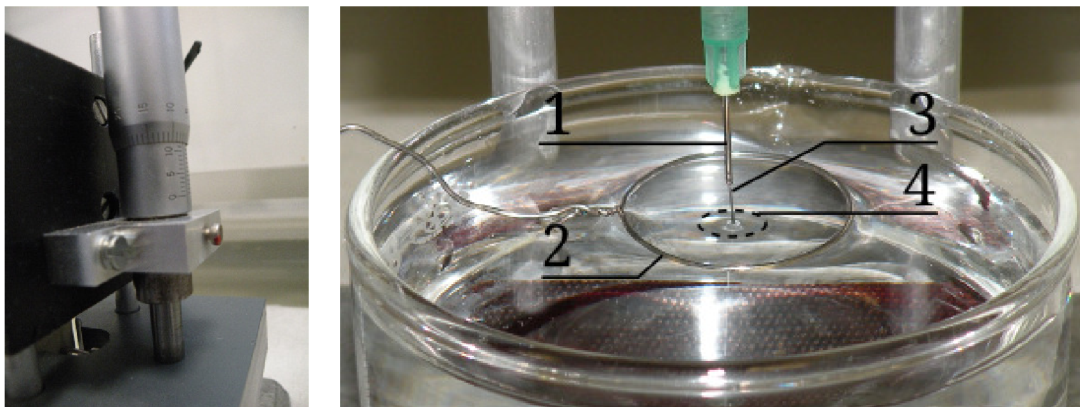

Figure 4.4: Details of the apparatus. On left side is the micrometer gauge. On the right side is a detail from the static electrochemical etching setup in figure 4.3. (1) hypodermic needle serving as a support for the tungsten wire, (2) stainless steel ring, (3) tungsten wire, (4) meniscus.

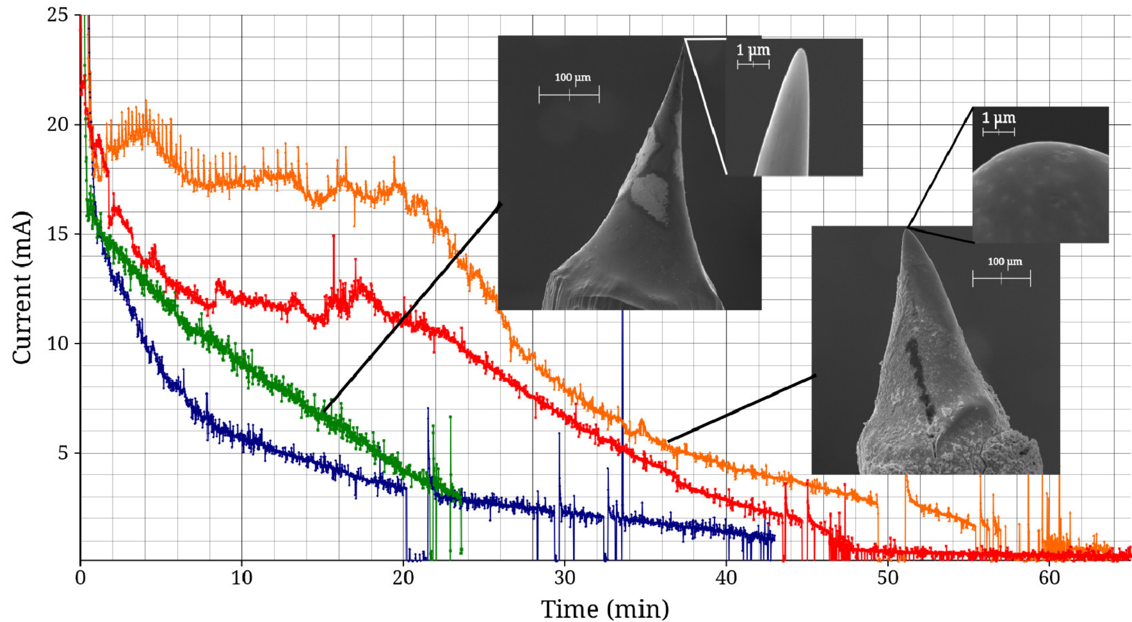

Figure 4.5: Etching of 300 μm tungsten wire in volatilised KOH at potential 12 V

It worked on basis of a built in threshold current control - the control setup has disconnected the circuit in case the current flow went under the bottom margin. The bottom margin of current flow was initially, after discussing [8], set to 2 mA.

The method for electrochemical tip sharpening was as follows

1. cut sufficiently long wire from the coil ($\sim$ 10 cm)
2. clean the cut wire in Aceton and then Isopropyl alcohol
3. put the wire inside of the holder, so that $\sim$ 5 mm stands out
4. immerse the wire 3 mm into the KOH with help of micrometer screw gauge
5. start the etching procedure and record the current against time
6. when the etched wire falls off (noticed by "stop process" in LABview), remove it from the electrolyte
7. remove remaining KOH with water
8. leave required length of the wire ($\sim$ 5 mm) and cut off the tip

When using two months old KOH, results were as shown in figure 4.5. All of these measurements had equal conditions and a 12 V potential was applied between the electrodes. Two of the tips have been analysed SEM and details of their shape and of their apexes have been added to the current against time data. It was quickly realised, that the etching process takes too long (according to literature [8, 33**?**]) and the KOH is already volatilised. Thus the two molar KOH has been again mixed and experiments started anew.

How the current changes in time for potentials $(12-6)$ V is shown in figure 4.6. For each potential was the etching process repeated approximately three times with all of the conditions held constant. The drop off time for each tip has then been taken out of the current-time measurement. Figure 4.7 shows the dependancy of a drop off time for each measured potential.

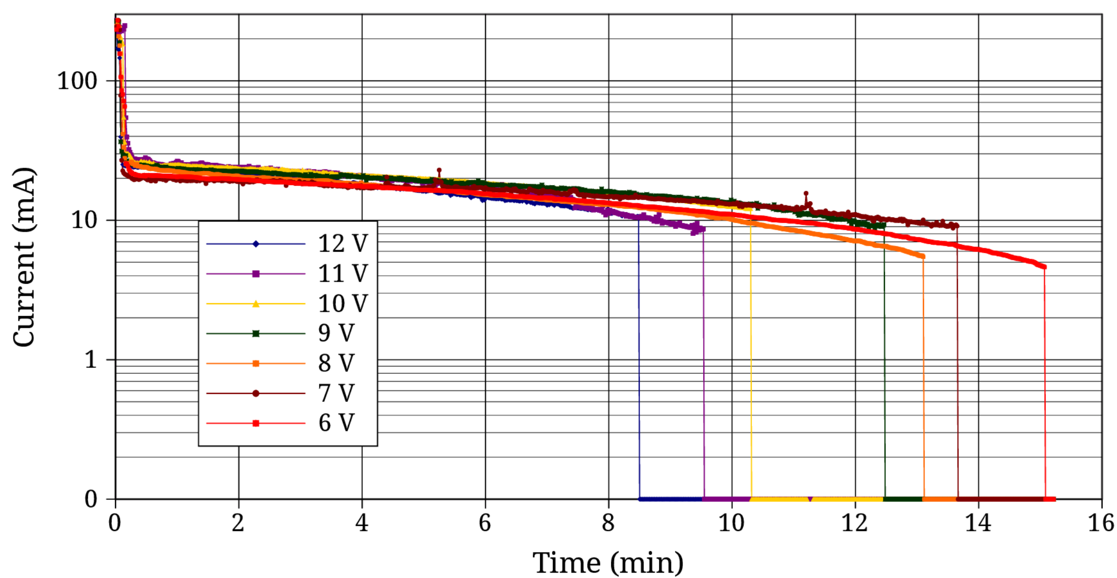

Figure 4.6: Etching with different potentials

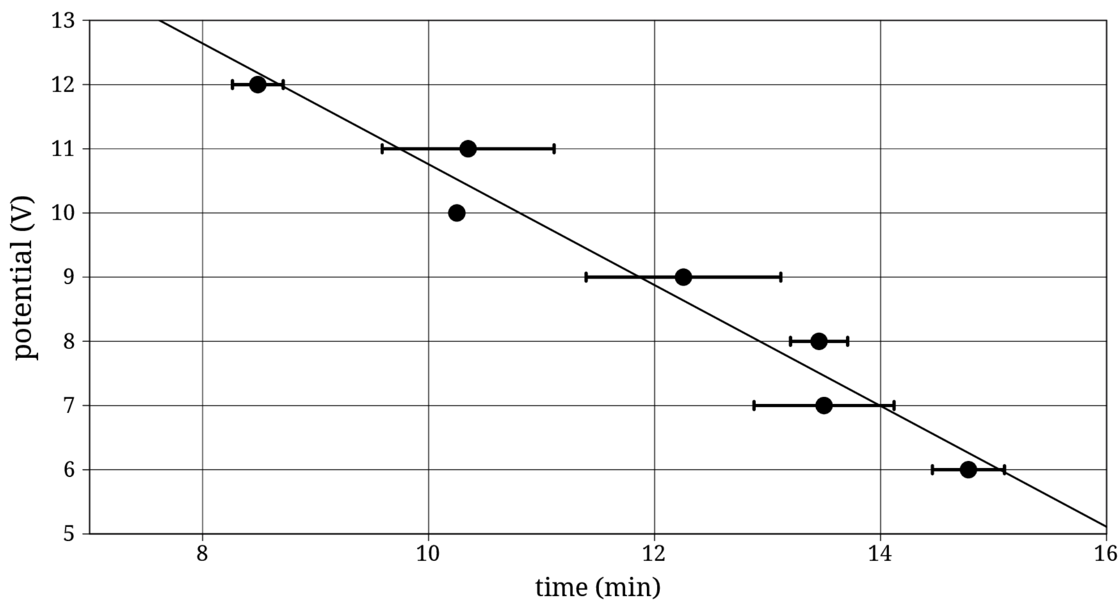

Figure 4.7: Potential versus time

It has been expected that the higher the potential between the tip and the electrolyte, the quicker the etching process. Reason for this assumption is that the velocity of the etching process is dependant upon the concentration of the constituent molecules. Their speed, since they are all charged particles, is in turn dependant upon the electrical field applied to them. Higher potential difference therefore concludes in quicker removal of tungsten from the wire. This assumption has been confirmed also by SEM images 4.9. It is further discussed in 4.1.2, page 25. Although all of the conditions were held constant for each potential, there are error bars, most significant for odd potentials. There are multiple reasons, which could describe this behaviour. Firstly, there has been no vibration damping. Since the meniscus has a very soft composition (due to surface tension), any vibration across the KOH surface could have caused a change in its placement on the tip. In this way either new parts of the wire had to be etched off or, if the meniscus moved downwards, less of the wire had to be etched off. Secondly, there have been bubbles of hydrogen (see equation 3.2, page 16) leaving the chemical reaction area. The H_2 molecules however did not always have the force to break the surface tension of the KOH and remained on site. This has retarded the speed of the reaction, again resulting in change of etching conditions. As was mentioned in section 3.3.1, page 16, this is the very reason why a dynamic method has been developed. As a part of this thesis, the setup for dynamic etching was prepared (see figure 4.8). However, no measurements were conducted until the deadline for this thesis because of a few minor problems. In the future, it may be interesting to finish this method off and compare the static and dynamic methods. Other reasons for the difference in drop off time for same potential would be angle distortion (when the wire was not perpendicular to the KOH surface) and continual volatilisation of KOH when the tips were being etched. It must be noted that etching of odd input potentials has taken place on a different day, with freshly mixed KOH.

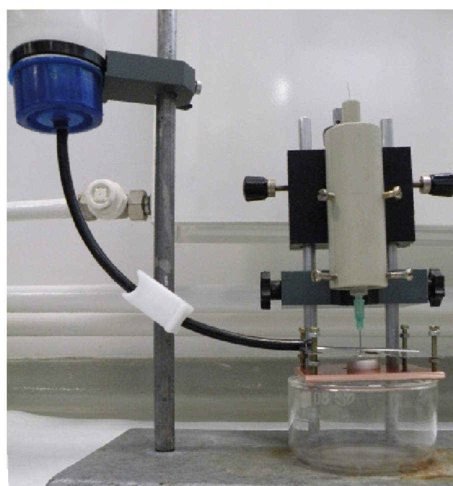

Figure 4.8: Setup for dynamic electrochemical etching. It was not in operation until the submission date of this thesis.

4.1.2 SEM images

SEM images of some of the etched tips were made in order to draw conclusions of their characteristics. Figure 4.9 compares the height of the tips etched at 12 V, 10 V, 8 V and 6 V potential and shows a detailed view of two apexes. Radius of curvature for both tips is in the order of $\sim 10^1$nm, which is comparable with the literature [5, 8, 33]. All of the SEM images were made by electrons with energy of 30 keV, in high vacuum.

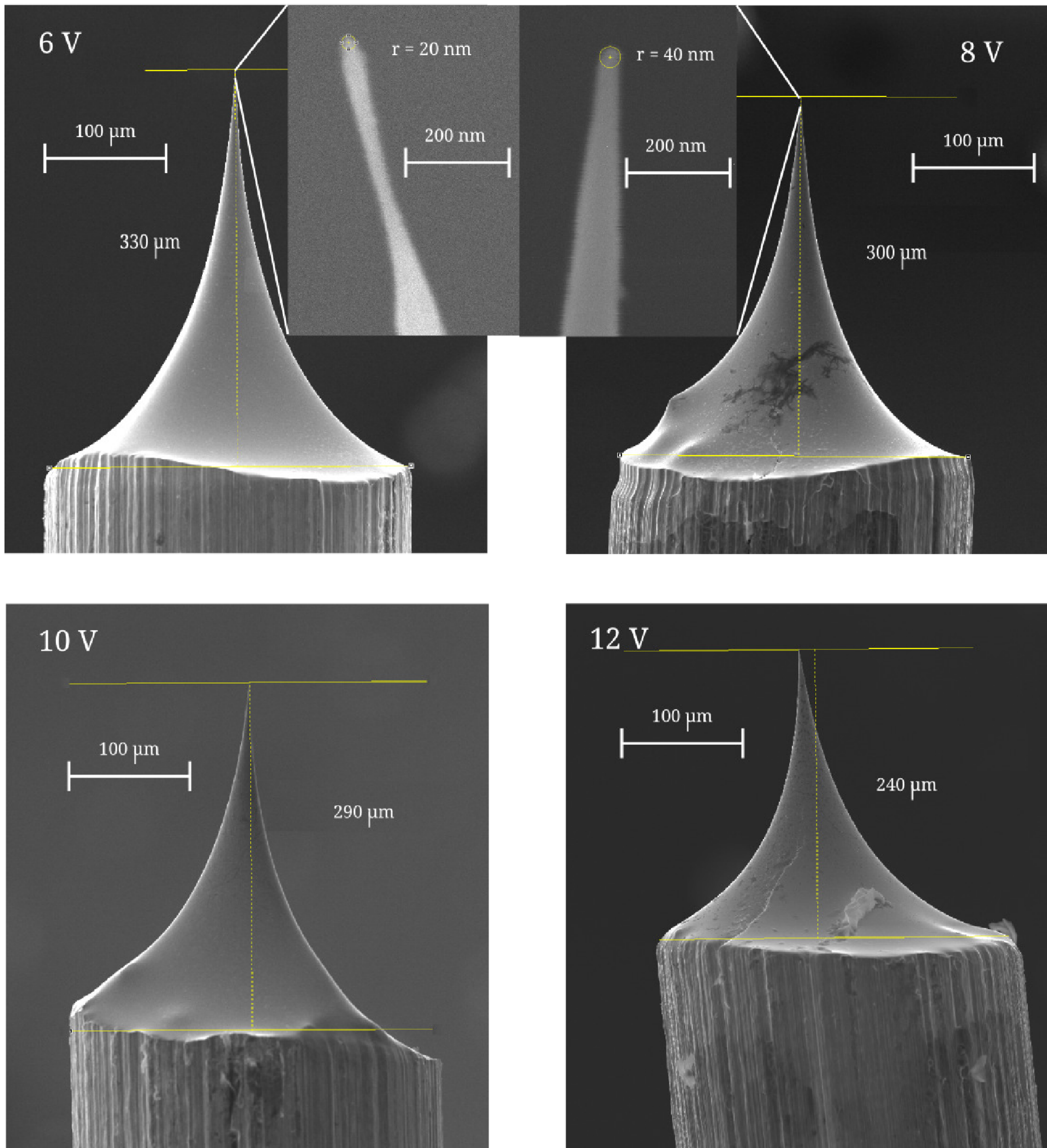

Figure 4.9: SEM images of four different tungsten tips with details of the apexes of two of them. The tips differ in etching potential, which in turn affected their length.

From these images it is clear that the higher the etching voltage, the shorter the tip length. Reason for this was already discussed in subsection 4.1.1, on page 23. A

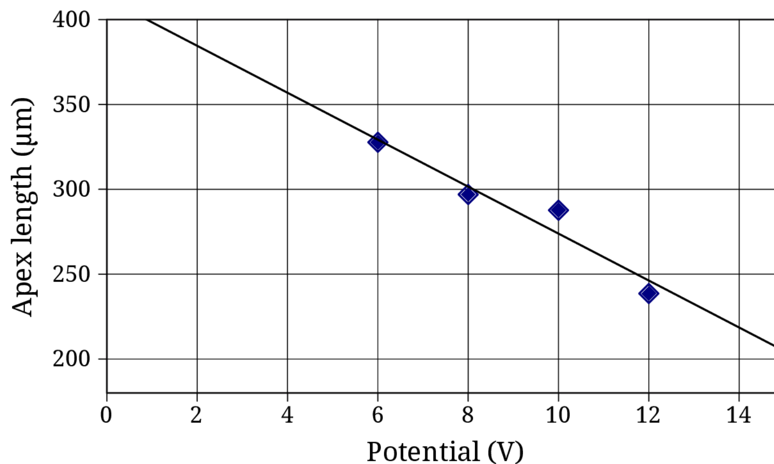

Figure 4.10: Analysis of lengths of apexes of four tungsten tips against the etching potential in static method.

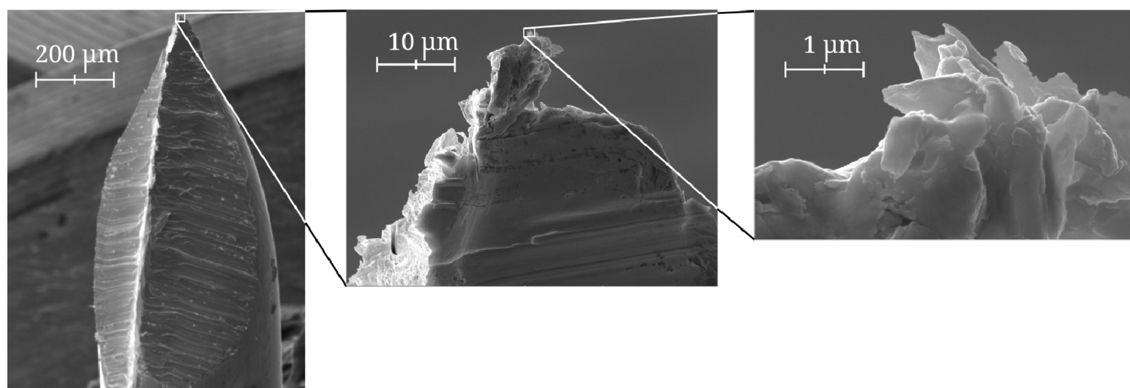

Figure 4.11: SEM analysis of a Pt/Ir cut tip

simple graph (Figure 4.10) shows a plot of this relation. The data are overlayed with a linear function, but it is expected that for zero potential will the length of the wire go to infinity and an asymtote could be also expected for infinite potential, because the wire would be immediately "etched off". These conclusions are not considering the complexity of the problem, they are merely pointing out that although the data seem to have linear dependancy, they are only a part of a larger function.

Figure 4.11 shows SEM images of a Pt/Ir cut tip (already mentioned in section 3.3). Detailed capture shows the apex of the tip is not clearly defined. Only a slight change in the tilt of the sample scanned by this tip would lead to electrons tunneling to the tip, thus resulting in noisy images. However, figure 4.22 proves that a cut tip can have resolution sufficient enough for distinguishing between atomic layers of carbon.

4.1.3 FIB sharpening

In previous sections was proved it is possible to electrochemically etch STM tips with radius of tens of nanometers. However, as was discused in section 3.1, an ideal STM tip would be terminated with a single atom. To get as close as possible to achieve this, tips discussed in subsection 4.1.1 were sharpened by Ga ion beam on Tescan®SEM-FIB combined microscope LYRA 3 FIB-FESEM. Its schematic view is shown in figure 4.1.3. This scheme pictures the angle between the FIB gun and

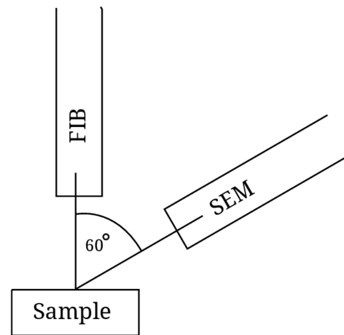

Figure 4.12: Schematic view of Tescan®SEM-FIB combined microscope LYRA 3 FIB-FESEM

the SEM, which could be also perceived from the figure 4.13. The working principle of FIB was mentioned in subsection 3.3.3, page 17. Connecting FIB and SEM gives the opportunity to watch macroscopic results of interactions between the ions and the substrate nearly in real time. All of the figures in this subsection have Ga^+ ions accelerated by the potential of 30 keV. Figures in this section have been acquired with the help of Ing. Tomáš Šamořil.

Figure 4.13 shows the first trial with FIB sharpening of etched tungsten tips. Ions used for bombardment were Ga^+. The figure on the left side shows the etched tungsten tip (etched at 8 V) and the picture in the middle shows a detail of its apex. Figure on the right shows the result of the Ga^+ ion bombardment. It was very

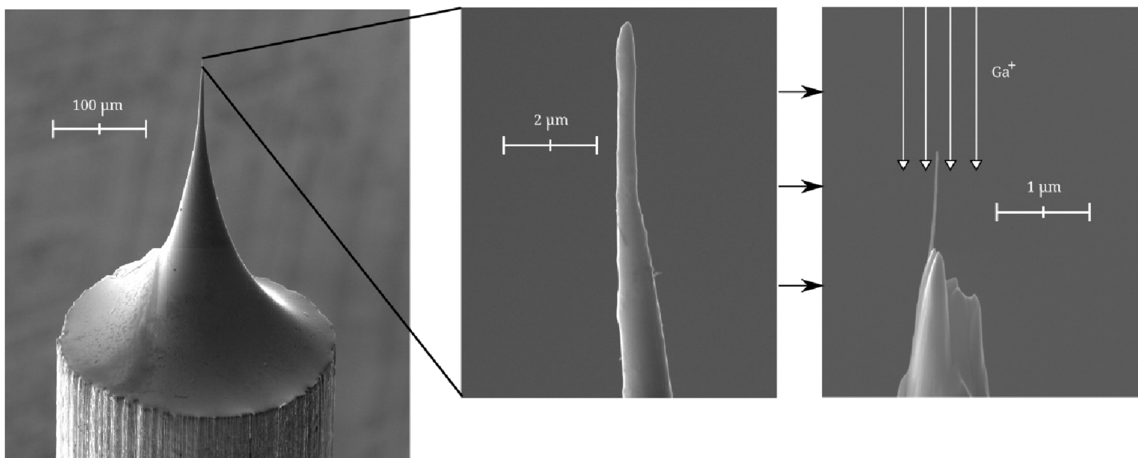

Figure 4.13: Etched tungsten tip sharpened by FIB.

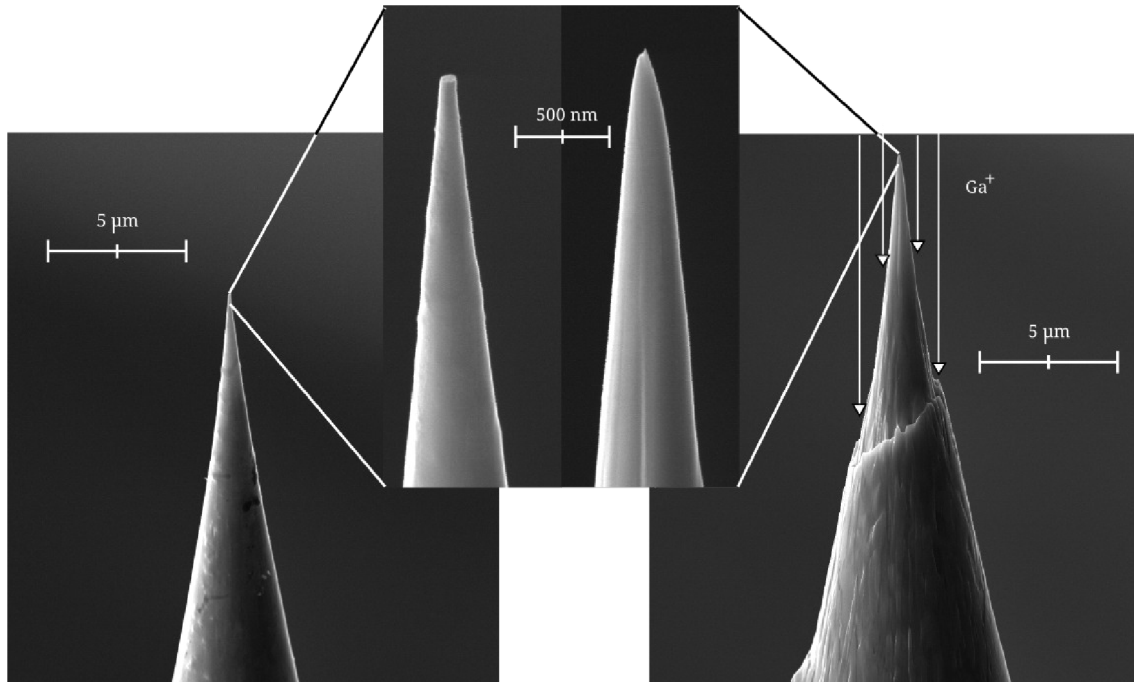

Figure 4.14: STM tip etched at 7 V, with the view field of 20 μm. STM tip etched at 7 V with the view field of 3 μm

surprising to see the remaining tungsten fiber with the apex radius of approximately 10 nm. To understand this phenomenon, new experiments have been undertaken.

Figure 4.14 shows the FIB sharpening of a tungsten tip etched at potential 7 V. The right picture clearly defines the area where the focused beam of Ga^+ was hitting the surface. The bombardment was done by continuous scanning over the specified area, in this case it was scanned over for $\sim$ 10 times by Ga^+ ions with energy of 30 keV. From this figure it is clear that the FIB sharpening is a very strong tool for the enhancement of UHV STM tip sharpness and through it of UHV STM measurements. Figure 4.15 aims to express the effect of Ga^+ bombardment on a cut tip. It was very hard to focus the ion beam right on the area that was supposed to be bombarded. The aim of the first bombardment was to hit the "highest" peak, which was unsuccessful. The second process was successful. The third aimed to scatter

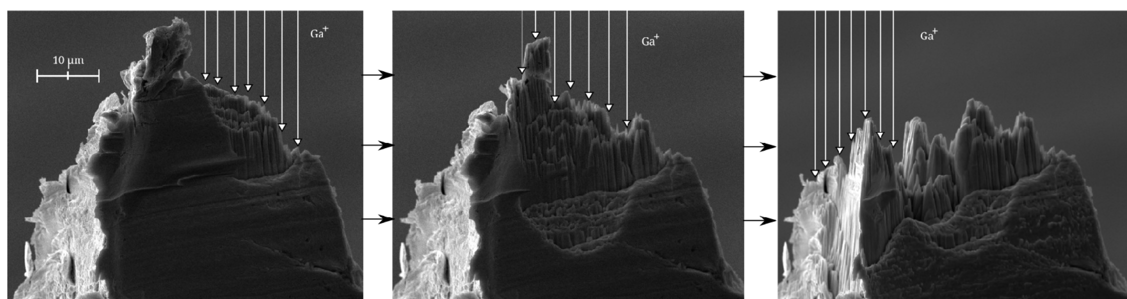

Figure 4.15: Three pictures show SEM view after three steps of GaN beam scattering of Pt/Ir. For original view refer to figure 4.11

off the left side of the apex, but missed and destroyed the apex. Three observations could be done, considering the sharpening of a Pt/Ir cut tip by FIB. Firstly, it is very hard to improve the apex of the cut tip, compared to etched one. Secondly, a Pt/Ir wire seems to consist of thin fibres and thirdly, Ga^+ ions are adsorbed to the surface of Pt/Ir (compare left and right pictures on figure 4.15).

4.1.4 UHV tip decontamination

Even though tungsten tips will be etched and then further sharpened by FIB, they will be transported into the UHV chambers for STM analysis through the atmosphere. This will lead to oxidation of tungsten and creation of native oxides WO_2 WO_3 on its surface [30]. There are various chemical methods how to remove it - for example in KOH or in Hydrogen Fluoride (HF). It should be noted that when making experiments in subsection 4.1.1, on page 19, it was noticed that if the tungsten wire was left in KOH, a reaction took place. Even without any potential applied to electrodes, the wire was after a few minutes very glossy. This was due to oxide removal.

The aim of this subsection was to propose an in-situ tungsten tip decontamination method through focused electron beam bombardment. This method could be therefore used to clean the tip even after the apex is clogged in the measurement without breaking the vacuum, which would in turn increase demands on design and materials used for it. This system exploits high melting point of tungsten (above 3000°C), which is higher than the melting point of its native oxides (∼1500°C) [1]. High density of electron flux will create a current flow through the tip, which would in turn heat up the tungsten wire. Since the tip is very sharp and the electrons will be focused into the very apex, the heating will be significant. In EOD®were created two designs of the geometry of the system (see figure 4.16). These designs aim to simulate real device that could be attached to already employed equipment in UHV chambers at IPE. Initially (left) was proposed a system with a source and a shield. The advantage of this setup was that the shield could be on a different potential compared to the source. The source consisted of an electrode and a tungsten filament and its purpose was to point the electrons emitted by the filament in the direction of the tip. The shield then served as a focusing lens, which would then bring the electrons to the tip. However it was realized that this setup would be very hard to design and manufacture. Thus the second design (right) was created. This

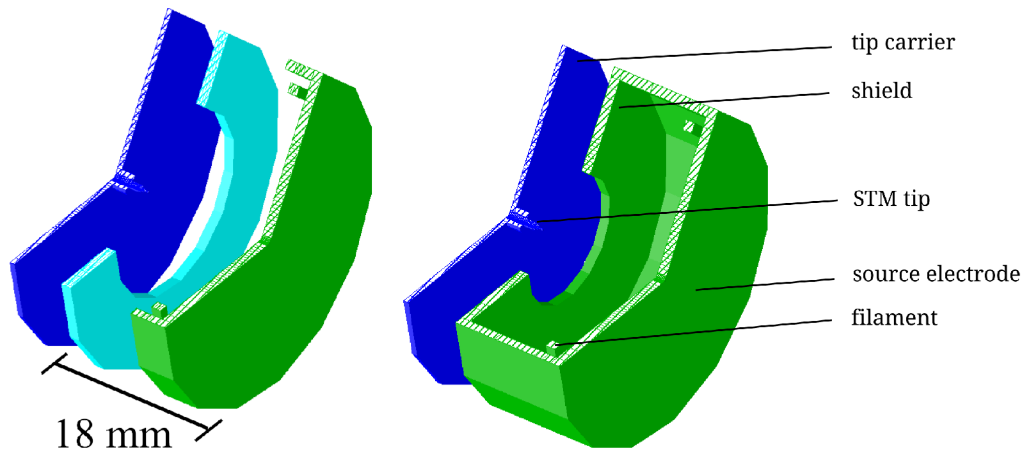

Figure 4.16: Analysed geometries of the system for tungsten tip decontamination. Simulations in EOD®. Left is the setup with separated shield and source, right is the compact setup.

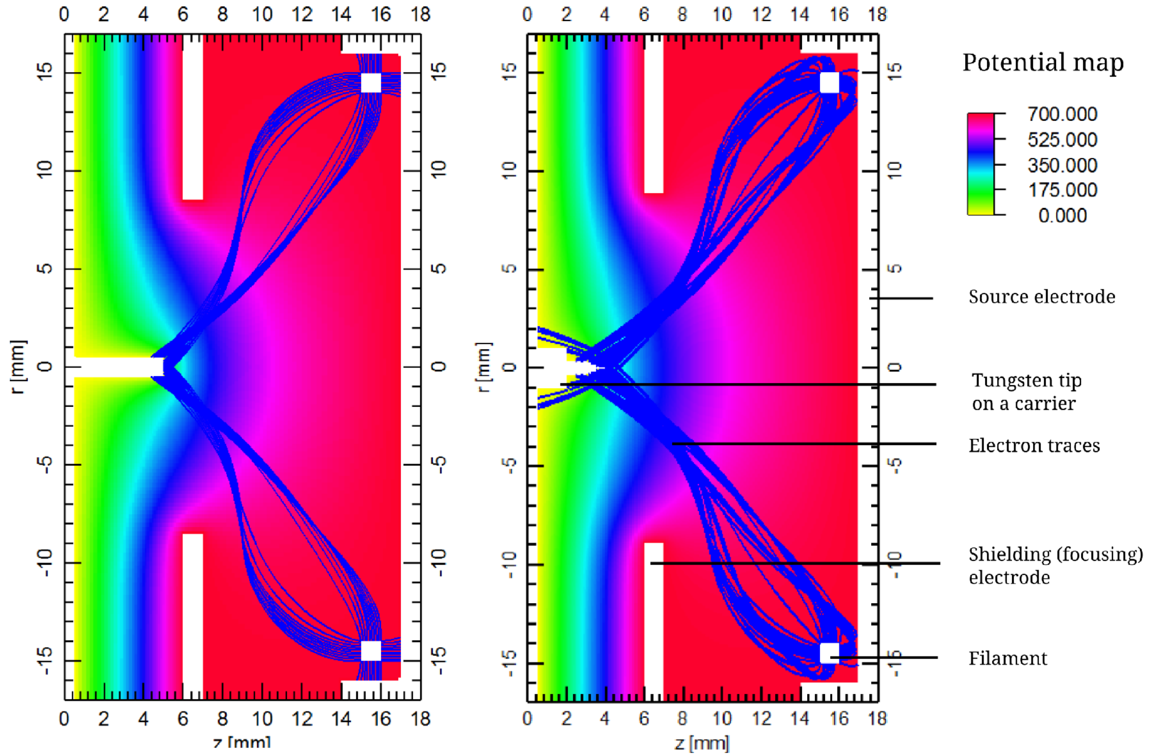

Figure 4.17: Simulations in EOD®

frame-up loses the advantage of shield and source on a different potential, but is much easier to manufacture.

In program EOD®were traced electrons from cathode (tungsten filament) to anode (STM tip). Considering the two distinct geometries, the variables in both cases were length of the shield and the accelerating potential. Figure 4.17 portraits electron traced in the first geometry. After several simulations it was clear that the shield does not have to be on different potential compared to the source of electrons (this argument is supported by figure 4.18). This figure shows another observation. The geometry of the tip plays a significant role on where will the electrons be focused to. Left picture shows a simplified design with electrons focused on the very end of the tip, whereas the picture to the right shows a more precise approximation of the tip in the carrier with constant variables. The beam of electrons is not focused anymore. It has not been understood why the electrons emitted from the side of the filament closer to the backplane do not trace into the tip in the picture on the left in figure 4.17, but they do in the picture in the right.

Figure 4.18 shows the connection between the accelerating potential and the length of the shield. The picture on the left has the same parameters as the picture on the right in figure 4.17, only the geometry has changed. The middle picture shows an attempt to focus the electrons by an increase in accelerating potential. This brings the electrons closer to the tip, but it is the change in the width of the gap in the shield that finally focuses the electrons onto the tip. Figure 4.19 shows detailed view of electron traces arriving at the tip. It can be seen that all of the emitted electrons are focused on the tip only.

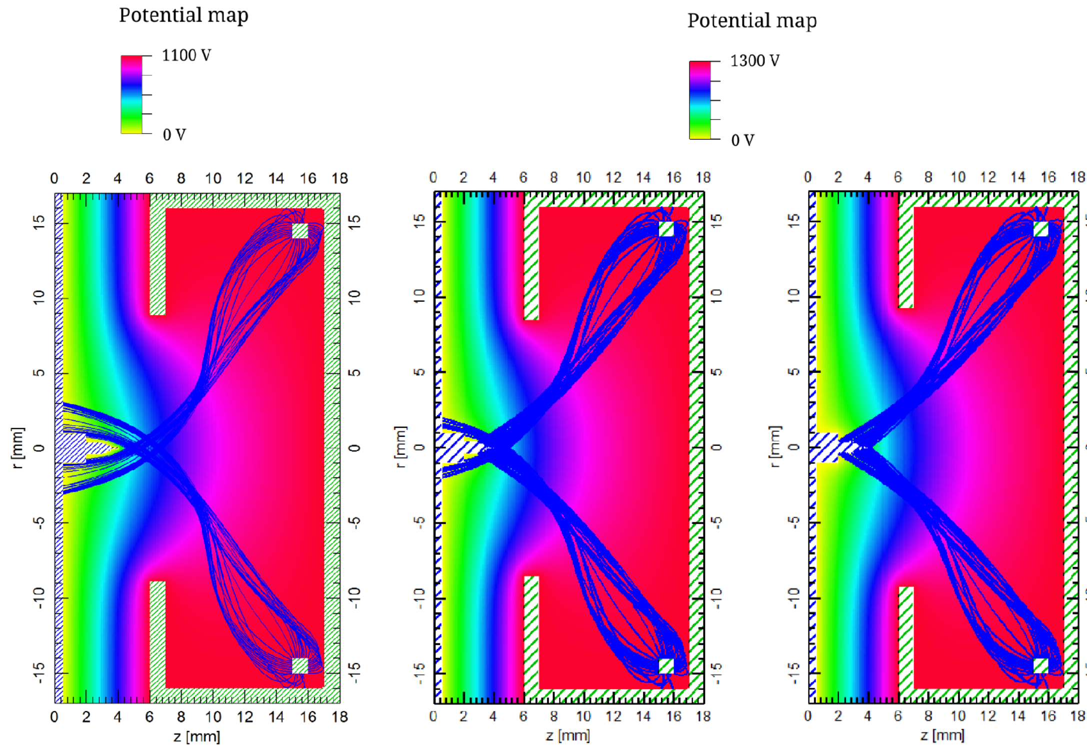

Figure 4.18: Simulations in EOD®

These simulations could be exploited when designing a device for STM tip decontamination compatibile with UHV equipment in the laboratory at IPE. Further information could be found in [11]. Simulations in [11] were done in SIMION®and include work with Richardson equation as a tool for calculation of the temperature of the tip dependant upon the current flow in the tungsten filament.

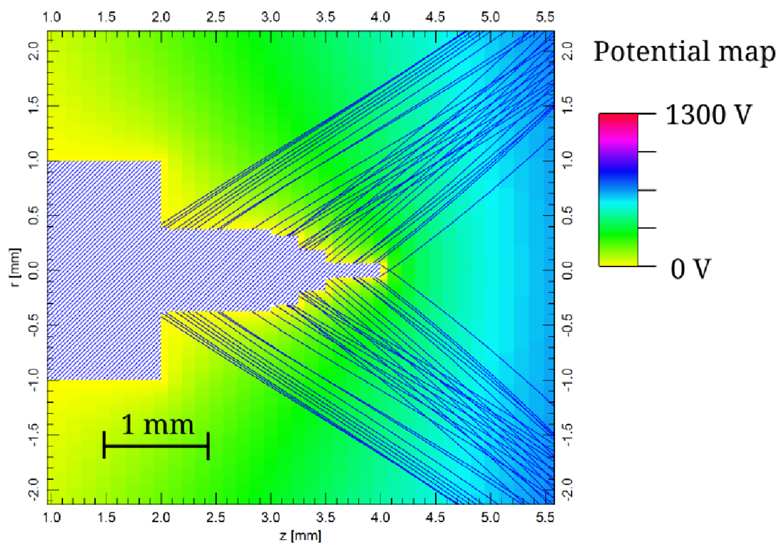

Figure 4.19: Simulations in EOD®, details

4.2 STM measurements

4.2.1 Etched and cut STM tips

According to studies of STM HOPG analysis in UHV, researchers are able to see atoms of C in HOPG and its lattice with tips with apex curvature radius ten to hundred times larger than those produced by electrochemical etching and FIB sharpening[5, 8]. Figures in this subsection have been post-processed in Gwyddion software and all of the measurements were done at room conditions.

The first acquired topographies are those in figure 4.20. The picture on the left presents tunneling current information from HOPG scanned over by a cut Pt/Ir tip and the picture on the right shows a zoomed view. The tip used for this measurement is shown in figure 4.11. Figure 4.21 portraits a difference between STM forward and

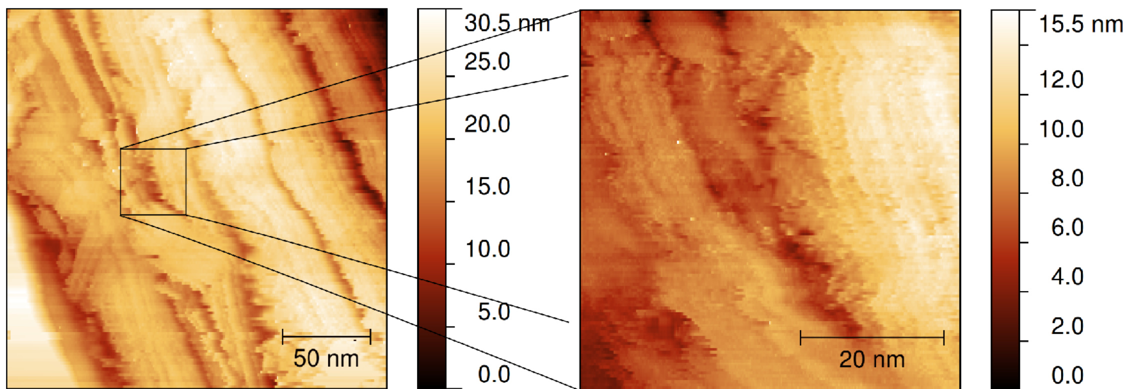

Figure 4.20: STM topography (constant tunneling current) from HOPG created with cut tip. View field of 212 nm and 52 nm, tunnel voltage 1.25 V, tunnel current 4 nA, gain 10.

backward scanning. The STM is sensitive to the shape of the apex, its symmetry and possible impurities on the sample. Therefore although the topographies are different, the figures are relevant. Figure 4.22 finally compares measurements of

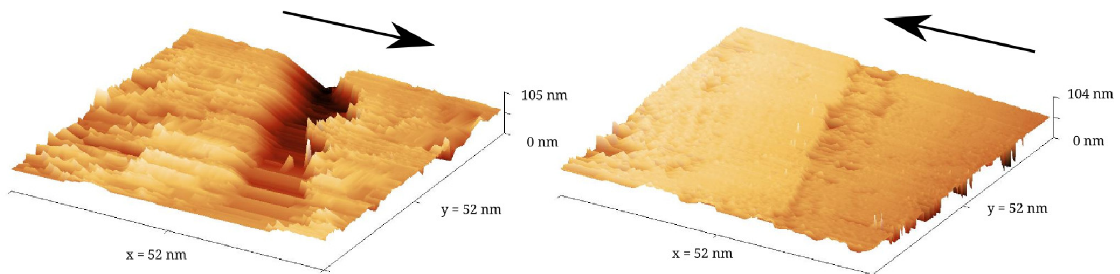

Figure 4.21: Comparison of forward and backward scanning. Information on topography (constant tunneling current) from HOPG measured with the same cut tip as in figure 4.20. View field of 52 nm, tunnel voltage 1.62 V, tunnel current 2.46 nA, gain 40.

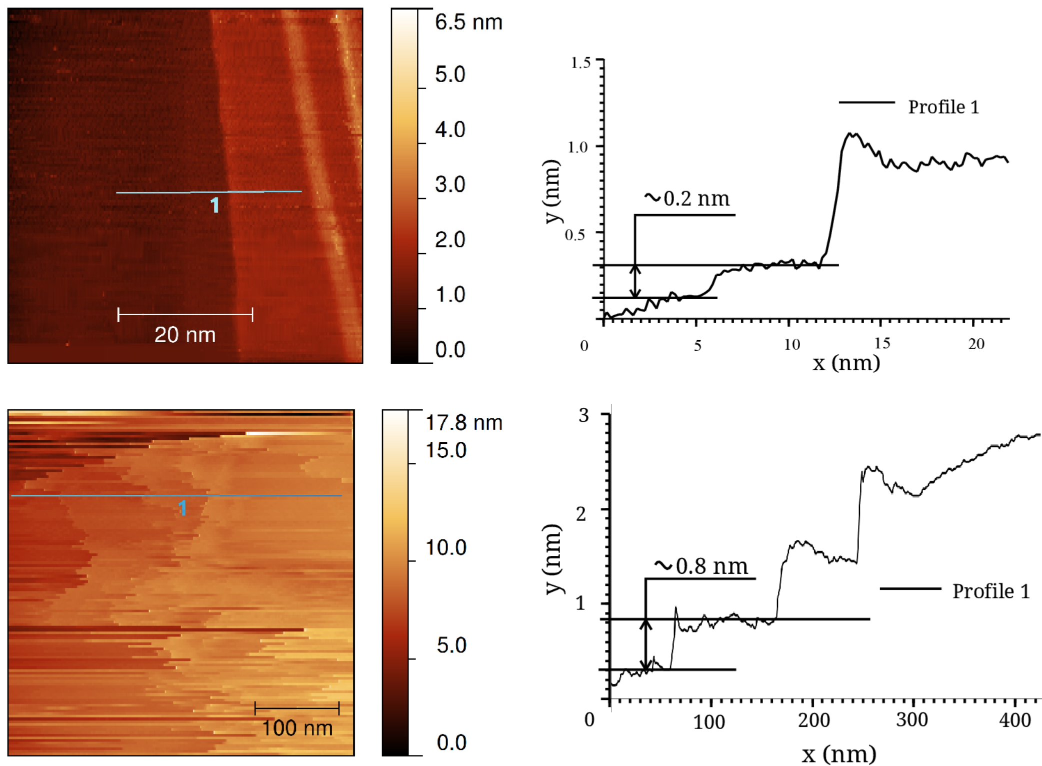

Figure 4.22: Terraces on HOPG measured by cut (top) and etched tungsten tips. For each, left is the STM image and right is the detail of the topography. Parameters of the top figure: view field of 52.3 nm, tunnel voltage 1 V, tunnel current 2.26 nA, gain 15.Parameters of the bottom figure: view field of 403 nm, tunnel voltage 0.56 V, tunnel current 2.97 nA, gain 19.

HOPG at room contidions with etched and cut STM tips. The top figure represents measurement of HOPG made by a cut tip. Here could be seen a monolayer of carbon. For better analysis has been done an extract of the topography. According to this measurement, the height of a carbon atomic layer is ~ 0.2 nm, which is in a good proximity to [6], where the distance between layers is defined to be 0.335 nm. This image is a courtesy of Zdeněk Nováček. On the other hand the measurement of HOPG terraces done by an etched tungsten tip did not show atomic monolayers. It was very hard to obtain resonable images and the best one is shown in the bottom part of the figure 4.22, along with a detail of its topography. It is hard to define how exactly the native oxides on tungsten tip affect the measurement, but after series of data collected was it clear that tungsten tips are for UHV use only.

4.2.2 Deposition of GaN and its analysis by STM

Gallium Nitride was already discussed in section 2.3, page 10. For this thesis it was decided to choose the deposition of GaN crystals on Silicon (Si) 7x7 (111) in antonin chambers 2.6.

The process consisted of three main steps. First was preparation of the Si substrate. It was cut into a (5x25)mm rectangle, placed into a sample carrier and heated up to 600 °C to clean it off the basic impurities, such as O, O_2, H_2O, N_2, organic compounds etc. However, when these compounds disintegrate, they leave bulk amorphous carbon in place. Annealing is a process that aims to remove it. It is an operation, during which the sample is held at 600 °C for 57 s and then suddenly heated up to the highest possible temperature below Si melting point (i.e. annealed) 1200 °C for 3 s. This procedure was repeated for approximately 20 minutes, until the total time of annealing reached ∼1 minute. An increase of pressure in the chamber was a sign that the oxides are being evaporated off the surface. After this follows continuous cooling of the sample from 600 °C to its deposition temperature of 300 °C. This leads to rearrangement of atomic layers near the surface of Si.

The second step was heating of the deposition cells. Cells used were UHV Evaporator, which is a commercial Ga effusion cell, and ion-atomic source. Both of them are described in section 2.2.4, page 7. The filament of the effusion cell had to be heated up slowly in order not to destroy it, culminating at flux 77 nA. Ion-atomic source was used to emit N^+ ions only. The reason why Ga atoms were emitted from the commercial cell was that it is able to supply Ga atomic beam with higher flux.

When both sample surface and deposition cells were prepared, deposition itself could have begun. Firstly, Ga atoms were deposited for approximately one hour, after them the N^+ ions for another hour. However, it is impossible to calculate the total dose of GaN deposition, because there were problems with measurement of N^+ ions current and also, the effusion cell did not work properly. The deposition was supposed to be repeated three times, but because of these problems, it was not. However, it was expected that the crystals would grow even though the procedure was problematic. Figure 4.2.2 shows an overview of an 403x403 nm^2 area on the sample analyzed by the STM, using a cut tip. There was an idea to try to compare the topographies of the sample in different potentials. The results are shown in figure 4.2.2. These three pictures (and a 3D view of the last one) apparently do not show any connection.

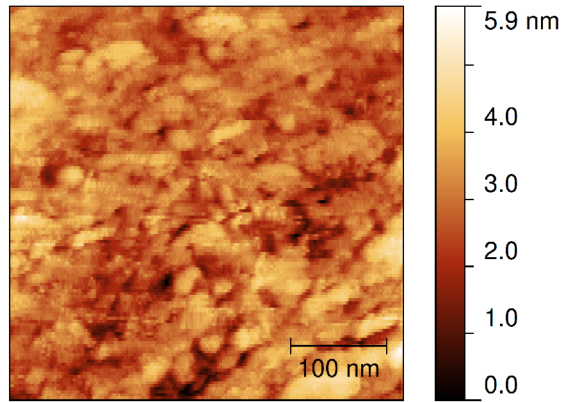

Figure 4.23: STM analysis of GaN deposition. View field of 403 nm, tunnel voltage 2.61 V, tunnel current 2.46 nA, gain 40.

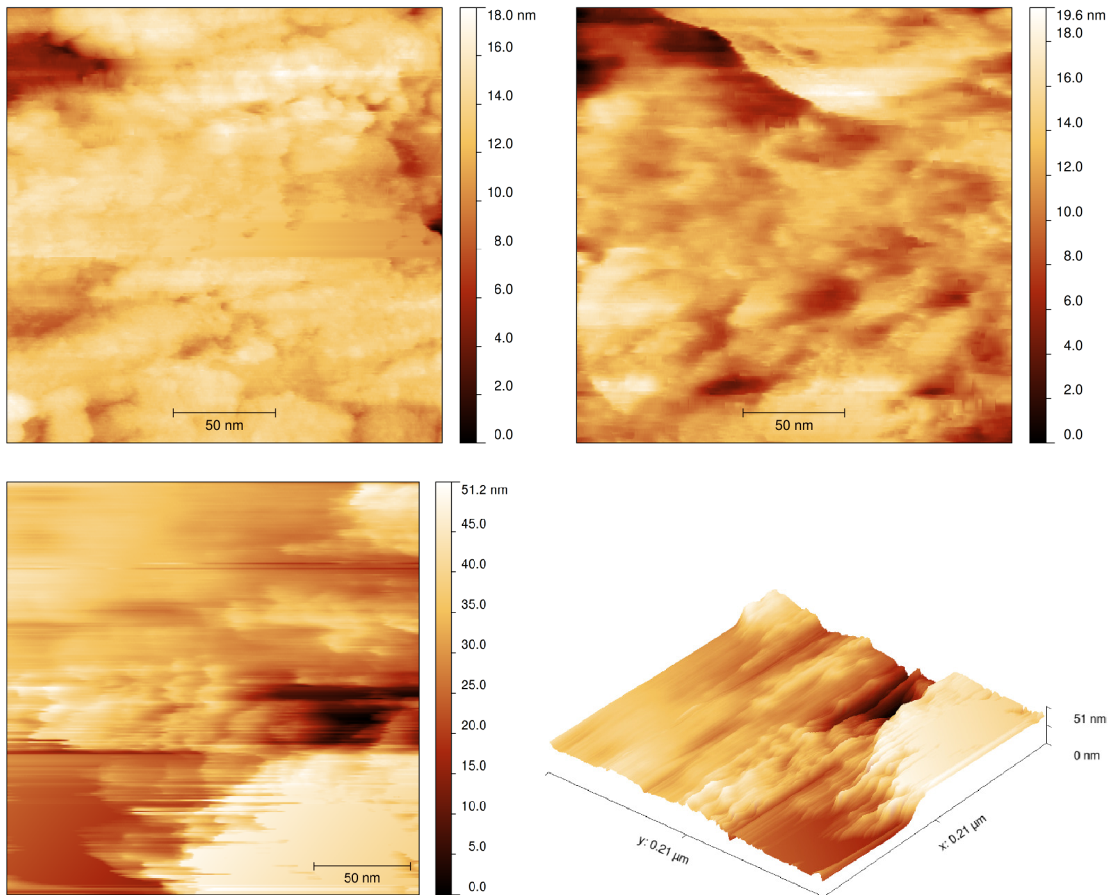

Figure 4.24: Change in topography due to change in potential: top left is a scan at tunnel voltage 2.61 mV, top right 1.62 mV, bottom left 0.62 mV (with larger range because of clarity). Bottom right is a 3D view of the topography inspected at lowest tunnel voltage. All figures share a view field of 212 nm, tunnel current of 2.46 nA and gain 40.

5 CONCLUSION

This thesis is focused on experiments connected to STM tip preparation with a strong emphasis on tungsten tips, which were supposed to be used in UHV. It was shown how it is possible to reproducibly etch very sharp tungsten tips.

A section on depostition of GaN crystals followed after the preparation of nanostructures was discussed in detail in the theoretical section. It was meant for these to be analyzed in UHV SPM, but the SPM head was not inside the UHV by the submission date of this thesis. Therefore, only STM measurements on air were performed. As predicted by the literature, tungsten tips did not give good results despite the fact that they were extremely sharp. Instead of them the sample was scanned by cut Pt/Ir tips, which does not oxidize on air, but can not compare in apex radius with electrochemically etched tips.

An apparatus for a static method of electrochemical etching was successfully improved. The improvement consisted of an amplifier and a software interface. Relations of drop off time dependent upon etching potential and the length of a tip against the etching potential were drawn. The SEM images of cut and etched tips were compared. An account for further enhancement of the sharpness of their apexes with FIB was also considered. It was found out that the cut tip can not be sharpened by FIB, whereas the FIB sharpening is very efficient for etched tips. The STM tip section was concluded with an outline of in-situ tungsten tip revitalization by focused electron beam.

Since a complex method for STM tips preparation has been proposed by this thesis, future developements could include utilization of these tips in UHV. Also, it would be interesting to find out how the flow of the electrolyte affects the properties of etched tips in the dynamic method. These data could then be compared with the data in this thesis. Finally, the simulations for the proposed in-situ tip decontamination could be used to design new equipment for the UHV chambers at IPE.

REFERENCES

[1] Melting points. `http://www.webelements.com`. Accessed: 04/05/2012.

[2] John R. Arthur. Molecular beam epitaxy. *Surface Science*, 500(1–3):189 – 217, 2002.

[3] J.R. Arthur. Surface stoichiometry and structure of gaas. *Surface Science*, 43(2):449 – 461, 1974.

[4] G. Binnig and H. Rohrer. Scanning tunneling microscopy. *Helvetica Physica Acta*, 55, 1982.

[5] H. Borque and R. M. Leblanc. Electrochemical fabrication of scanning tunneling microscopy tips without an electronic shut-off control. *Rev. Sci. Instrum.*, 66(3):2695–1902, 1995.

[6] LeMay Brown and Bursten. *Chemistry: the central science*. Pearson Prentice Hall, Upper Saddle River, NJ, 2008.

[7] O'Mara William C. *Handbook of semiconductor silicon technology*. Noyes Publications, Park Ridge, N.J, 1990.

[8] I. Ekvall et al. Preparation and characterization of electrochemically etched W tips for stm. *Measurement Science and Technology*, 10:11–18, 1999.

[9] C.T. Foxon, M.R. Boudry, and B.A. Joyce. Evaluation of surface kinetic data by the transform analysis of modulated molecular beam measurements. *Surface Science*, 44(1):69 – 92, 1974.

[10] H. Freller and K.G. Günther. Three-temperature method as an origin of molecular beam epitaxy. *Thin Solid Films*, 88(4):291 – 307, 1982.

[11] M. Geryk. *Konstrukce ultravakuové komory pro sledování struktury povrchů pevných látek metodou LEED a STM/AFM*, Brno University of Technology, Faculty of Mechanical Engineering, 2001. Diploma Thesis.

[12] J. E. Greene et al. The role of low-energy ion/surface interactions during crystal growth from the vapor phase. *Cambridge Journals*, 75, 1986.

[13] S. Heike, Y. Wada, and T. Hashizume. Correlation between tip-apex shape and surface modification by scanning tunneling microscopy. *Journal of Applied Physics*, 86(8):4220–4224, 1999.

[14] J. P. Ibe et al. On the electrochemical etching of tips for scanning tunneling microscopy. *Journal of Vacuum Science and Technology A*, 8, 1990.

[15] F. A. Stevie L. A. Giannuzzi. *Introduction to focused ion beams instrumentation, theory, techniques, and practice*. Springer, New York, 2005.

[16] K. M. Lang et al. Conducting atomic force microscopy for nanoscale tunnel barrier characterization. *Review of Scientific Instruments*, 75:2726–2731, 2004.

[17] B. Lencová and J. Zlámal. A new program for the design of electron microscopes. *Physics Procedia*, 1(1):315 – 324, 2008. Proceedings of the Seventh International Conference on Charged Particle Optics (CPO-7).

[18] H. Sitter M. A. Herman. *Molecular Beam Epitaxy - Fundamentals and Current Status*. Springer Series in Materials Science.

[19] J. Mach. *Vývoj a aplikace UHV zařízení pro depozice tenkých vrstev (atomární a iontové svazkové systémy)*, Brno University of Technology, Faculty of Mechanical Engineering, 2010. Ph.D. Thesis.

[20] J. Mach et al. An ultra-low energy (30-200 eV) ion-atomic beam source for ion-beam-assisted deposition in ultrahigh vacuum. *Review of Scientific Instruments*, 82(8):1–7, 2011.

[21] D. Marton. *Film Deposition from Low energy Ion Beams, very Low Energy Ion surface interactions*. Wiley.

[22] E. Meyer, H.J. Hug, and R. Bennewitz. *Scanning Probe Microscopy: The Lab on a Tip*. Advanced Texts in Physics. Springer, 2012.

[23] Nanosurf AG. *Operating Instructions Easyscan 2*.

[24] T. Novák. *Rekonstrukce iontového děla a jeho aplikace pro tvorbu tenkých vrstev a nanostruktur*, Brno University of Technology, Faculty of Mechanical Engineering, 2011. Bachelor's Thesis.

[25] T. Němeček. *Užití kovových materiálů pro selektivní růst*, Brno University of Technology, Faculty of Mechanical Engineering, 2008. Diploma Thesis.

[26] A. J. Ptak. *Growth Kinetics and Doping of Gallium Nitride Grown by rf-Plasma Assisted Molecular Beam Epitaxy*, West Virginia University, 2001. Ph.D. Thesis, `http://www.scribd.com/doc/36784460/Ptak-Thesis`.

[27] F. Rinaldi. *Basics of Molecular Beam Epitaxy*, University of Ulm, 2002. Technical Report, `http://www-opto.e-technik.uni-ulm.de/forschung/jahresbericht/2002/ar2002_fr.pdf`.

[28] T. Schimmel, L. Eng, H. Fuchs, and M. Luxsteiner. Mechanical nanostructuring of wse2 with the stm - tip shape dependence and writing techniques. *Annales de Chimie-Science des Materiaux*, 17(3-4):205–216, 1992.

[29] John T. Tate and P. T. Smith. The efficiencies of ionization and ionization potentials of various gases under electron impact. *Phys. Rev.*, 39:270–277, Jan 1932.

[30] Z. L. Wang W. Zhou. *Scanning microscopy for nanotechnology: techniques and applications*. Springer, New York London, 2007.

[31] S. Watanabe, M. Aono, and M. Tsukada. Effects of the tip shape on scanning tunneling microscope images - 1st-principles calculations. *Journal of Vacuum Science and Technology B*, 12(3):2167–2170, 1994.

[32] H. Ximen. Microfabrication of afm tips using focused ion and electron beam techniques. *Ultramicroscopy*, 1992.

[33] R. Zhang and D. G. Ivey. Preparation of sharp polycrystalline tungsten tips for scanning tunneling microscopy imaging. *Journal of Vacuum Science and Technology B: Microelectronics and Nanometer Structures*, 14(1):1–10, 1996.

[34] D. Škoda. *Vývoj a testování UHV-kompatibilního mikroskopu AFM/STM*, Brno University of Technology, Faculty of Mechanical Engineering, 2001. Diploma Thesis.